Effects of temperature and carbon source on the isotopic fractionations associated with O_2 respiration for $^{17}O/^{16}O$ and $^{18}O/^{16}O$ ratios in *E. coli*

Daniel A. Stolper[a] Woodward W. Fischer[b] Michael L. Bender[cd]

Abstract

$^{18}O/^{16}O$ and $^{17}O/^{16}O$ ratios of atmospheric and dissolved oceanic O_2 are used as biogeochemical tracers of photosynthesis and respiration. Critical to this approach is a quantitative understanding of the isotopic fractionations associated with production, consumption, and transport of O_2 in the ocean both at the surface and at depth. We made measurements of isotopic fractionations associated with O_2 respiration by *E. coli.* Our study included wild-type strains and mutants with only a single respiratory O_2 reductase in their electron transport chains (either a heme-copper oxygen reductase or a *bd* oxygen reductase). We tested two common assumptions made in interpretations of O_2 isotope variations and in isotope-enabled models of the O_2 cycle: (*i*) laboratory-measured respiratory $^{18}O/^{16}O$ isotopic fractionation factors ($^{18}\alpha$) of microorganisms are independent of environmental and experimental conditions including temperature, carbon source, and growth rate; And (*ii*) the respiratory 'mass law' exponent, θ, between $^{18}O/^{16}O$ and $^{17}O/^{16}O$, $^{17}\alpha = (^{18}\alpha)^{\theta}$, is universal for aerobic respiration. Results demonstrated that experimental temperatures have an effect on both $^{18}\alpha$ and θ for aerobic respiration. Specifically, lowering temperatures from 37 to 15 °C decreased the absolute magnitude of $^{18}\alpha$ by 0.0025 (2.5‰), and caused the mass law slope to decrease by 0.005. We propose a possible biochemical basis for these variations using a model of O_2 reduction that incorporates two isotopically discriminating steps: the reversible binding and unbinding of O_2 to a terminal reductase, and the irreversible reduction of that O_2 to water. Finally, we cast our results in a one-dimensional isopycnal reaction-advection-diffusion model, which demonstrates that enigmatic $\delta^{18}O$ and $\Delta^{17}O$ variations of dissolved O_2 in the dark ocean can be understood by invoking the observed temperature dependence of these isotope effects.

Keywords: Triple oxygen isotopes, Aerobic respiration, Dissolved oxygen

1. Introduction

The isotopic composition and concentration of O_2 in the atmosphere and oceans are used in the Earth sciences to quantify net and gross photosynthesis at global and local scales in both the present and the past (e.g., Bender and Grande, 1987, Bender, 1990, Quay et al., 1993, Bender et al., 1994b, Luz et al., 1999, Luz and Barkan, 2000, Luz and Barkan, 2011, Nicholson et al., 2014); as tracers of ocean circulation (e.g., Kroopnick and Craig, 1976, Bender, 1990, Maier-Reimer, 1993, Levine et al., 2009); for the construction of ice-corechronologies (e.g., Bender et al., 1994a, Petit et al., 1999); and to reconstruct historical changes in the hydrological cycle (Bender et al., 1994b, Severinghaus et al., 2009). Additionally, the isotopic

composition of O_2 has been used to study the physiology of plants (e.g., Guy et al., 1987, Ribas-Carbo et al., 1995), microorganisms (Helman et al., 2005), and humans (Epstein and Zeiri, 1988, Zanconato et al., 1992) as well as in studies of enzyme-specific processes (e.g., Tian and Klinman, 1993, Cheah et al., 2014). In all such applications, a quantitative understanding of how the isotopes of oxygen are fractionated by these chemical and physical processes is necessary. Here, we evaluated how growth temperature and the organic carbon substrate control the isotopic fractionations associated with O_2 reduction during aerobic respiration in the gammaproteobacterium *Escherichia* coli. Our objectives were to improve the constraints on O_2 isotopic fractionations during aerobic respiration and to develop a process-level understanding of what parameters, if any, modulate these fractionations.

1.1. Background on the isotopic composition and biogeochemistry of O_2 in the oceans and atmosphere

The isotopic composition of O_2 is described using delta (δ) notation[1] where tropospheric air is defined to have $\delta^{18}O$ and $\delta^{17}O$ values equal to 0‰. Isotopic fractionations are denoted using alpha notation where

(1)18αi-j=18Ri18Rj.

In Eq. (1), $^{18}R = [^{18}O]/[^{16}O]$ (brackets denote concentrations), and *i* and *j* are two different phases or species (e.g., O_2 and H_2O). A similar notation is used for $^{17}O/^{16}O$ fractionations. ε notation is commonly used in biogeochemical studies and is related to $^{18}\alpha$ such that $^{18}\varepsilon_{i-j} = 1000 \times (1 - {}^{18}\alpha_{i-j})$. For aerobic respiration, unless otherwise noted, species *i* is the O_2that is respired relative to the larger, remaining pool of O_2 (species *j*). Most processes in nature fractionate $^{17}O/^{16}O$ ratios relative to $^{18}O/^{16}O$ ratios following 'mass-law' relationships (Miller, 2002) such that:

(2)1000×lnδO171000+1=1000×λ×lnδO181000+1.

Any deviation from the measured $\delta^{17}O$ value relative to that expected based on the $\delta^{18}O$ value and the chosen slope, λ, is encapsulated by a sample's $\Delta^{17}O$ value (Miller, 2002), where:

(3)ΔO17=1000×lnδO171000+1-1000×λ×lnδO181000+1.

Note that the mass-law slope λ for aerobic respiration is sometimes defined in oxygen-isotope studies as γ (Luz and Barkan, 2005). Luz and Barkan (2005) recommended that γbe used when referring to irreversible, kinetically controlled processes such as O_2 reduction during respiration in a closed system. We additionally used θ to describe the direct relationship between $^{18}\alpha$ and $^{17}\alpha$ (Dauphas and Schauble, 2016):

(4)17αi-j=18αi-jθ.

We note that others have substituted the symbol β for θ (Young et al., 2002).

The $^{18}\varepsilon$ value for aerobic respiration in the upper oceans is thought to range from 18 to 22‰ (Quay et al., 1993, Bender et al., 1994b, Hoffmann et al., 2004, Hendricks et al., 2005, Luz and Barkan, 2011). Aerobic respiration across a range of organisms has been found to exhibit a λ of 0.518 (Luz and Barkan, 2005). We followed previous workers (e.g., Luz and Barkan, 2005) in using $\lambda = 0.518$ as the reference λ value in calculations of $\Delta^{17}O$ [Eq. (3)]. Aerobic respiration in a closed system (i.e., no mass transfer between the system and outside world) does not change $\Delta^{17}O$ values of O_2 if it exhibits a λ of 0.518.

During oxygenic photosynthesis, Cyanobacteria express negligible isotopic fractionations for the production of O_2 via the oxidation of H_2O ('water splitting') such that $^{18}\varepsilon_{O2\text{-}H2O} = 0$‰; i.e., the $\delta^{18}O$ values of photosynthesized O_2 and the source H_2O are thought to be identical (within 0.5‰ of each other; Guy et al., 1987, Stevens et al., 1975, Guy et al., 1993, Helman et al., 2005, Eisenstadt et al., 2010). Measureable isotopic fractionations have been observed for some algae in which the $\delta^{18}O$ value of newly photosynthesized O_2 is up to 7‰ higher than of the source H_2O; this has been attributed to an unknown reductive process hypothesized to occur in algal cells after O_2 formation (Eisenstadt et al., 2010).

The absence of substantial oxygen isotopic fractionations during photosynthetic water oxidation combined with a respiratory $^{18}\varepsilon$ value of ~18–22‰ is generally considered to be the main reason that O_2 in the troposphere is elevated in $\delta^{18}O$ relative to seawater by 23.8‰ (the "Dole" effect; Kroopnick and Craig, 1972, Horibe et al., 1973, Barkan and Luz, 2005). In the oceans, addition of photosynthetic O_2 changes both the $\delta^{18}O$ and $\Delta^{17}O$ of dissolved O_2towards the oxygen isotope composition of seawater. Seawater is lower in $\delta^{18}O$ than tropospheric O_2 by ~24‰ but higher in $\Delta^{17}O$ by ~0.3‰ when using $\lambda = 0.518$ (Luz and Barkan, 2005).

In the surface oceans, $\delta^{18}O$ and $\Delta^{17}O$ values of O_2 depend on the combined effects of photosynthesis and respiration. Photosynthesis can cause supersaturations of O_2 in the upper oceans, leading to $\delta^{18}O$ values of dissolved O_2 that are lower (Bender and Grande, 1987) and $\Delta^{17}O$ values that are higher (Luz and Barkan, 2000) than the values expected when dissolved O_2 and gaseous O_2 are in chemical and isotopic equilibrium with each other. These patterns enable the use of dissolved O_2 concentrations to calculate net photosynthetic rates (i.e., the total photosynthetic rate minus the total aerobic respiration rate). When combined with $\delta^{18}O$ and/or $\Delta^{17}O$ values, they allow the calculation of gross (i.e., total) photosynthetic rates (Bender and Grande, 1987, Craig and Hayward, 1987, Luz and Barkan, 2000). In the dark oceans, i.e., below the mixed layer and the photic zone (typically >60–100 m in open ocean basins), respiration causes the concentration of O_2 to decline and $\delta^{18}O$ values of dissolved O_2 to increase. If no mixing occurs between water masses, respiration takes place in a closed system and leaves $\Delta^{17}O$ values of dissolved O_2unchanged (Fig. 1).

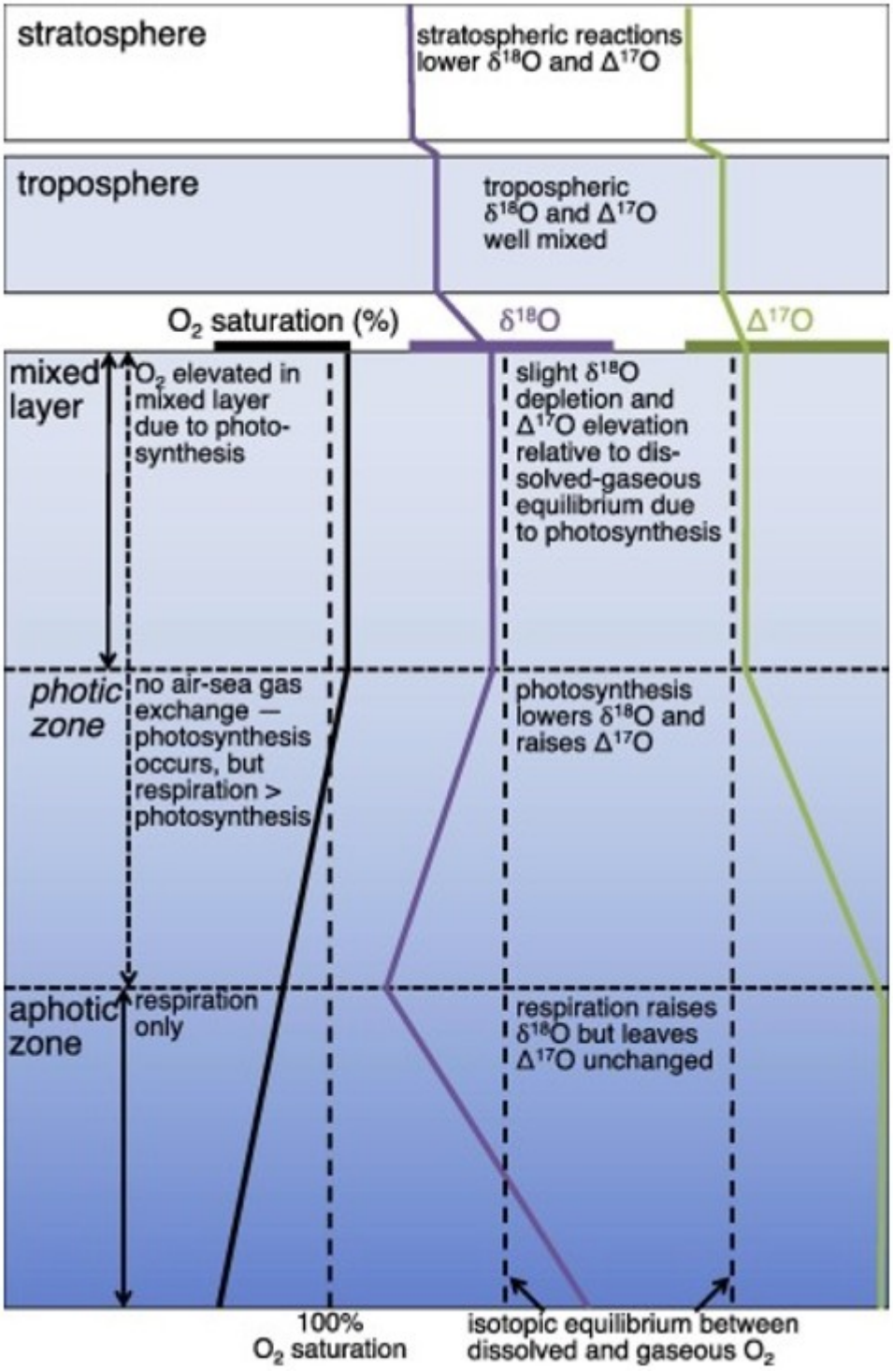

Fig. 1. Schematic of oceanic processes controlling the concentration and isotopic composition of O_2 in the atmosphere and oceans.

1.2. Current questions on processes that control the isotopic composition of O_2

In the dark oceans, fractionation factors for respiration have been estimated using mass-balance models coupled to measurements of O_2 concentrations and $\delta^{18}O$ values. These models vary in complexity from one-box representations of the dark oceans to three-dimensional global circulation models (Kroopnick and Craig, 1976, Bender, 1990, Maier-Reimer, 1993, Levine et al., 2009). For waters with small or moderate changes (<50%) in O_2concentrations relative to saturation with air, measured and modeled values for $\delta^{18}O$ of dissolved O_2 in the dark ocean are in agreement using respiratory $^{18}\varepsilon$ values determined previously (18–22‰). However, in waters with larger O_2 concentration changes (decreases of greater than 50% vs. saturation with air), observed $\delta^{18}O$ values of dissolved O_2 are generally lower than models predict when using $^{18}\varepsilon$ values of 18–22‰ (Bender, 1990).

Two causes are generally invoked to explain the lower-than-expected $\delta^{18}O$ values of O_2 in the dark ocean. In the first, low respiratory fractionations ($^{18}\varepsilon \sim 10‰$) are invoked. To date, however, no microorganisms have been found that produce such small fractionation factors during aerobic respiration. In the second explanation, mixing between water masses with different dissolved O_2 concentrations leads to lower $\delta^{18}O$ values than are obtained during closed-system O_2 consumption (Bender, 1990). Models that incorporate this mixing can replicate the $\delta^{18}O$ values of O_2 dissolved in the dark ocean using respiratory $^{18}\varepsilon$ values of 18-22‰. But they require water masses to exist with low O_2 concentrations (<10% of air saturation) and $\delta^{18}O$ values ~20‰ higher ($\delta^{18}O > 40‰$) than the highest $\delta^{18}O$ value of dissolved O_2 ever observed in the oceans ($\delta^{18}O \sim 20‰$; Bender, 1990, Maier-Reimer, 1993, Quay et al., 1993, Levine et al., 2009). Consequently, it remains uncertain what processes control the $\delta^{18}O$ values of O_2 in the dark ocean.

$\Delta^{17}O$ values of dissolved O_2 have been proposed to be unaffected by respiration (Luz and Barkan, 2011). That $\Delta^{17}O$ values are unaffected during aerobic respiration of O_2 is supported by the observation that all studied aerobically respiring organisms share the same (within error) mass-law slope of $\lambda = 0.518$ (Luz and Barkan, 2005). Note that λ values for respiration by single-celled organisms (both prokaryotes and eukaryotes), which are responsible for 90–95% of all respiration in the open ocean (del Giorgio and Duarte, 2002), have been measured for only three organisms: 2 Cyanobacteria (*Synechoycystis* and *Synechococcus*; Helman et al., 2005) and a heterotrophic bacterium (T10) isolated from the freshwater Lake Kinnert, Israel (Helman et al., 2005, Luz and Barkan, 2005). Thus, whether λ is truly constant amongst a wide variety of microorganisms remains an open question.

If λ is invariant across different aerobic organisms, then it follows that the $\Delta^{17}O$ value of dissolved O_2 in seawater in a closed system should never be below the $\Delta^{17}O$ value for equilibrium between O_2 dissolved in water vs. in air, which is between 0.005 and 0.018‰ (Keedakkadan and Abe, 2015). Interestingly, some samples from the dark oceans have negative $\Delta^{17}O$ values —as much as 0.05‰ lower than that expected for air-saturated waters

(Hendricks et al., 2005). Pointing to the non-linearity of mixing of $\Delta^{17}O$ values, Nicholson et al. (2014) showed that negative $\Delta^{17}O$ values of O_2 are possible if mixing of water masses with strongly differing $\delta^{18}O$ values of O_2 occurs. However, their example calculation required water masses to be present with $\delta^{18}O$ values of dissolved $O_2 \sim 45‰$ higher than the maximum values ever observed in the ocean. Consequently, we consider that the origin of $\Delta^{17}O$ values of O_2 in the dark ocean that are lower than that for equilibrium with the atmosphere remains an open question.

1.3. This study

Much of our understanding of what controls $\delta^{18}O$ and $\Delta^{17}O$ values of O_2 in nature are based on laboratory experiments of aerobic respiration and photosynthesis. A key assumption of these experiments is that observations made in the laboratory under one set of growth conditions (e.g., temperature, light levels, etc.), are relevant for that organism under all conditions and thus can be extrapolated to the environment. However, demonstrations of the correctness of this assumption are lacking. We tested this assumption by growing heterotrophic bacteria under a range of experimental conditions. Specifically, we grew *E. coli*in the laboratory at various temperatures and using different carbon sources. Our results showed that the temperature of the experiment influences expressed $^{18}\varepsilon$, λ, and θ values. Below we explored why temperature may influence the expressed isotopic fractionations using a simple mathematical model of isotopic fractionation of O_2 reduction during aerobic respiration. Finally, we examined these results in the context of oceanographic processes including mixing, advection, and respiration and demonstrate that these results help explain the low $^{18}\varepsilon$ values for aerobic respiration observed in the dark oceans.

2. Methods

2.1. Cultures, growth conditions, and sampling procedures

Pure cultures of *E. coli* NCM and mutants of *E. coli* K-12 were used to study isotopic fractionations associated with aerobic respiration. Wild-type *E. coli* possesses three O_2reductases: a low-O_2-affinity A-family heme-copper O_2 reductase (Han et al., 2011) and two high-O_2-affinity *bd* O_2 reductases. In order to test for possible enzyme-specific differences in expressed isotopic fractionations, we measured oxygen isotopic fractionations in mutant K-12 strains that each possess only one of these O_2 reductases. Cultures were grown in autoclaved minimal medium with the following salt additions: 2.5 g/L NaCl, 13.5 g/L K_2HPO_4, 4.7 g/L KH_2PO4, 0.8 g/L Na_2SO4, 0.1 g/L $MgSO_4 \cdot 7H_2O$, and 0.535 g/L NH_4Cl. After autoclaving, we added filter-sterilized solutions of 0.5 ml/L 1% vitamin B1, 0.1 ml/L 1 M $CaCl_2$, and 0.2 ml of trace element solution (Hahnke et al., 2014). Filter-sterilized solutions (4.7 ml/L of a 10% solution) of glucose, acetate, or glycerol were added to the medium as carbon sources following autoclaving. Glycerol was always the carbon source when the experimental temperature was varied. Autoclaving the carbon source along with the salt solution was initially attempted. However, abiotic

control experiments demonstrated that autoclaving the carbon source resulted in products that consumed O_2. Media was prepared in 5 L glass bottles and equilibrated with the atmosphere for at least two days while the media was stirred using a sterilized magnetic plastic stir bar. Equilibrations were conducted with a loosely fitted sterilized cap on the glass bottle that allowed for the maintenance of sterility and gas transport into and out of the headspace of the bottle.

Cells were grown in 500 ml Wheaton bottles. We added 0.5–1 ml of culture grown overnight (optical densities at 660 nm of between 0.5 and 1.5 measured on a ThermoFisher Scientific Evolution 220 spectrophotometer) to a bottle and then poured fresh media on top of this until the bottle was filled to the brim. A sterilized 30 mm butyl stopper was used to stopper the bottle (using a sterilized needle to eliminate any air during stoppering) and crimped. The bottles were then incubated between 15 and 37 °C depending on the experiment in a thermostated shaker (New Brunswick Scientific Excella E24 Shaker) at 175–200 rpm. Samples were removed from the incubator at discrete time points and siphoned into pre-evacuated 500 ml bottles poisoned with 200 ml of saturated $HgCl_2$ solution (dried down before being evacuated) with a single O-ring stopcock (Louwers-Hapert) following Emerson et al. (1995), such that ~250 ml of liquid were introduced into the bottles. Following this, samples were placed on a rotating drum to equilibrate gaseous and dissolved species for at least 3 hr. Liquid was transferred from inverted bottles to an evacuation flask, leaving behind a small residual of liquid (a few milliliters).

2.2. Gas extraction and purification

The 500 ml bottles containing the residual gas from the experiments (with a few milliliters of liquid remaining) were placed into mixture of ethylene glycol and water cooled to −40 °C using dry ice. They were then attached to a custom-made automated gas chromatographyline described in Blunier et al. (2002). Samples were frozen onto the first molecular sieve trap for 43 minutes. The gas chromatograph was operated at 35 °C with a helium flow rate set to 11 ml/min. After purification of O_2 and Ar from other gases, samples were frozen onto molecular sieves (type 5A, Davison Chemical) that had been preheated under vacuum at 200 °C for at least one hour. Samples were frozen onto the sieves for 20 min at liquid nitrogen temperatures. Sieves with samples were heated at 100 °C for at least one hour, and introduced into the mass spectrometer.

2.3. Mass spectrometry and precision

$\delta^{18}O$ and $\Delta^{17}O$ values were measured on a ThermoFinnigan Delta^{Plus} XL isotope-ratio mass spectrometer housed at Princeton University in the Department of Geosciences. External precision (one standard deviation [σ]) was determined from replicate measurements of O_2dissolved in deionized, poisoned water equilibrated with the atmosphere ($n = 14$). External precisions for $\delta^{18}O$, $\Delta^{17}O$, and $\delta O_2/Ar^2$ were 0.050, 0.008, and 0.8‰

respectively. Details of the mass spectrometry including information on precision and accuracy are given in Appendix A.1.

2.4. Calculation of fractionation factors and mass-law slopes

Values for $^{18}\alpha$ were calculated assuming the experiments followed a Rayleigh fractionationprocess such that:

(5)ln1000+δ18OO2timepoint1000+δ18OO2initial=18α-1×lnO2timepointO2initial.

In Eq. (5), 'time point' refers to a sample measured at a known time after the start of the experiment (the 'initial' time point) and [O_2] refers to the concentration of O_2. We did not measure the concentration of O_2 directly. Instead we calculated the relative change in the O_2concentration using $\delta O_2/Ar$ measurements under the assumption that the concentration of Ar did not change over the course of the experiment. Under this assumption, the following is true:

(6)1000+δO2/Artimepoint1000+δO2/Arinitial=O2timepointO2initial.

The mass-law slope (λ) describing the relationship between $\delta^{17}O$ and $\delta^{18}O$ values was found using the following equation:

(7)ln1000+δ17OO2timepoint1000+δ17OO2initial=λ×ln1000+δ18OO2timepoint1000+δ18OO2initial.

We calculated the value of θ [see Eq. (4)] using the following equation (derived in Angert et al., 2003):

(8)θ=lnλ×18α-1+ 1ln(18α).

Errors for θ were calculated based on the propagation of error through Eq. (8). Further details on how these fits were performed are given in Appendix A.2.

3. Results

3.1. Examples from a specific experiment

Before discussing trends in $^{18}\varepsilon$ and θ based on all of the experiments, we first present the results from an experiment to illustrate the nature of the data and data analysis. The selected experiment is the one with the largest number of time points measured in a single experiment ($n = 11$), and the largest change in dissolved O_2 concentrations (which fell to 21% of the starting concentration). In Fig. 2A, the change in $1000 \times \ln([\delta^{18}O_{O2\ time\ point}/[\delta^{18}O_{O2\ initial}])$ is plotted vs. the fraction of initial O_2 remaining. The fit (by linear regression) of these data to the line given by Eq. (5) is also shown, along with the residuals of the fit in Fig. 2B. The fit is robust ($r^2 = 0.9998$); however the standard deviation of the residuals is 0.14‰ (Fig. 2B) and is thus worse than our external reproducibility for individual $\delta^{18}O$ measurements of dissolved O_2 (±0.05‰, 1σ; see above). We took this to indicate that some level of additional noise beyond measurement precision is

introduced into the experiments—e.g., that fractionation factors vary subtly between bottles with cultures grown and killed at different time points in the experiment. Experiments with less consumption of O_2 (<50% of starting O_2 consumed) typically showed less scatter about the fitted line.

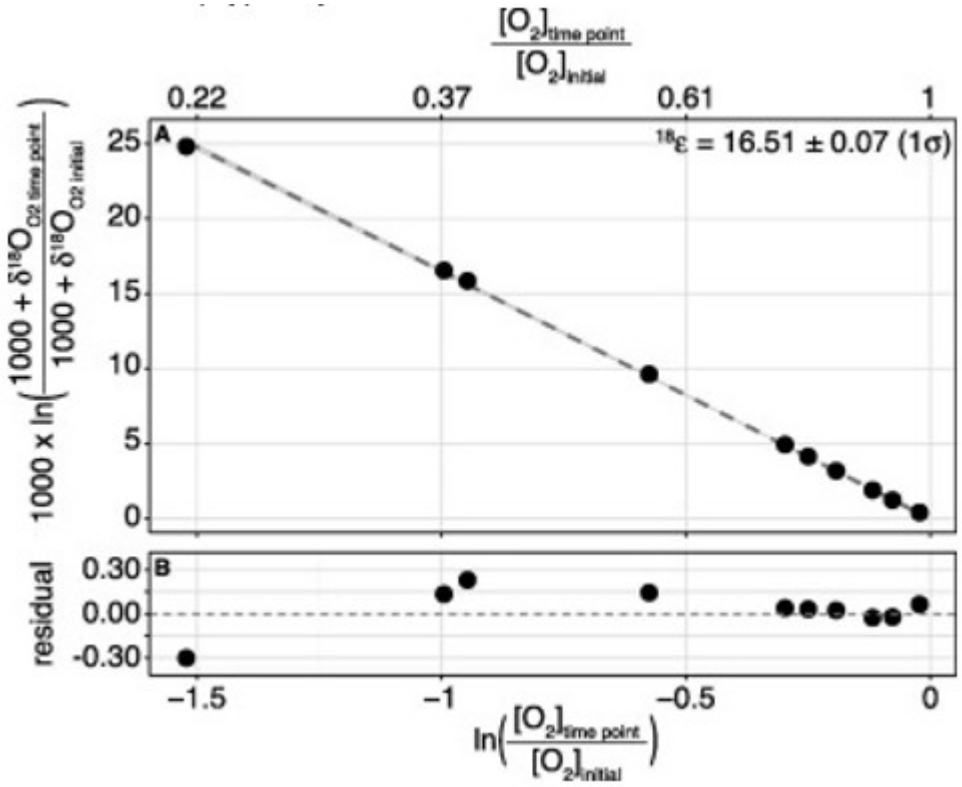

Fig. 2. An example of ^{18}O data from a 37 °C respiration experiment using glycerol as the carbon source. Data were plotted against the natural logarithm of the fraction of initial O_2 remaining (top) or the natural logarithm of the fraction (bottom). (A) $\delta^{18}O$ of O_2 vs. the natural logarithm of the fraction of O_2 remaining. Note the $\delta^{18}O$ data are normalized so that the initial data point in which no consumption has occurred is defined to have value of 0‰. This data point (not shown) lies at the origin, and the line is forced through this point (see Section A2). The dashed line is a fit to the data using Eq. (5). The light grey shading is the 95% confidence interval of the fit. The derived value for $^{18}\varepsilon$ is given along with 1σ error bars. (B) Residuals of the fit of the data vs. Eq. (5). Analytical error bars are smaller than the size of the points.

The relationship between $\delta^{18}O$ and $\delta^{17}O$ (in logarithmic form relative to the initial media value) is given in Fig. 3A and the residuals of the fit of this data to Eq. (7) are given in Fig. 3B. The data are also well fit by the line described in equation (7) ($r^2 > 0.9999$). In Fig. 3B, all residuals to the fit are within 2 standard errors of the external precision of the measurement (±0.008‰, 1σ).

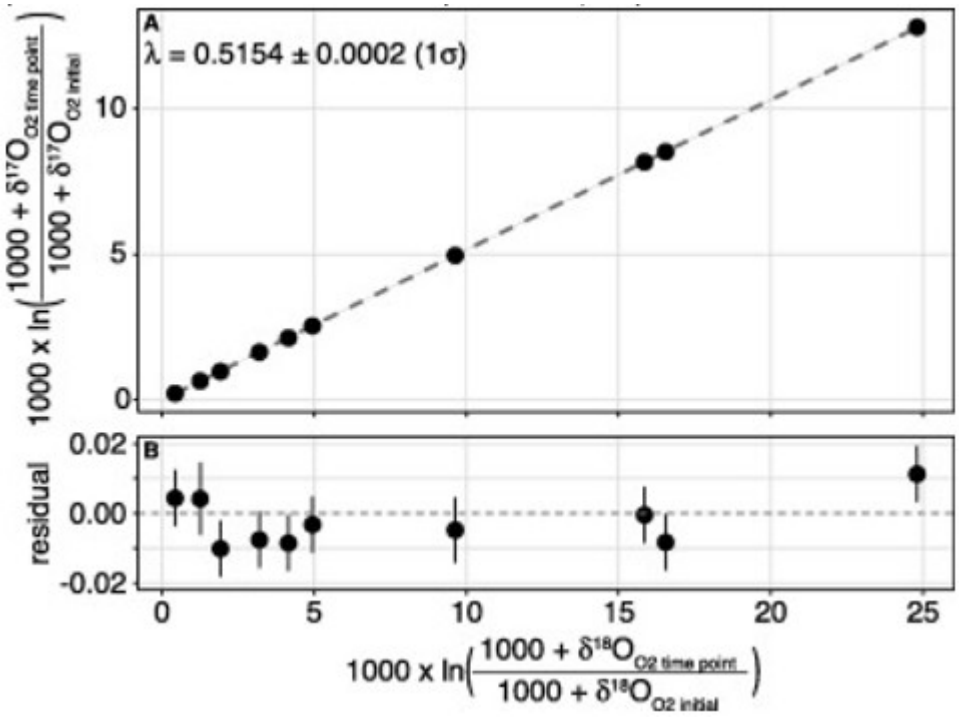

Fig. 3. ^{18}O and ^{17}O isotopic data from a 37 °C respiration experiment using glycerol as the carbon source (same experiment as Fig. 2). (A) $\delta^{18}O$ vs. of $\delta^{17}O$ (in logarithmic form). Note that the $\delta^{18}O$ and $\delta^{17}O$ data are normalized so that the initial data point in which no consumption has occurred is defined to have value of 0‰ for both. The dashed line is a fit to the data using Eq. (2). The slope of the line is λ as given in Eq. (2). The 95% confidence interval of the fit is too narrow to be seen. The derived value for λ is given in the upper right-hand corner. Error bars of points are smaller than the size of the points. (B) Residuals of the fit of the data vs. Eq. (2). Error bars are either the 1σ external reproducibility of the $\Delta^{17}O$ measurements (0.008‰), or the 1σ precision of the specific data point, whichever is larger.

3.2. Experimental reproducibility

The precisions for $^{18}\varepsilon$ and λ (and therefore θ) for a given experiment were estimated based on quality of the fit of the regressions. We additionally examined our experimental reproducibility by replicating the 37 °C and 15 °C experiments with glycerol as the carbon source using a new starting culture, new media, etc. We chose these experimental temperatures as they yielded the maximum and minimum $^{18}\varepsilon$ and θ values for wild-type *E. coli* NCM. The replications were performed 54 days apart for the 37 °C experiment, and 51 days apart for the 15 °C experiment.

For the 37 °C experiments, $^{18}\varepsilon$ values were measured to be 16.5‰ ± 0.07 (1σ) and 16.4‰ ± 0.05 (1σ). For the 15 °C experiments, $^{18}\varepsilon$ values were measured to be 14.4‰ ± 0.05 (1σ) and 13.9‰ ± 0.07 (1σ). These yielded a pooled standard deviation of 0.26‰ (1σ; i.e., the standard deviation based on data from both experiments; McNaught and Wilkinson, 1997). We considered this to be a conservative estimate of the true reproducibility of the determined $^{18}\varepsilon$ values for a single experiment.

For the 37 °C experiments, λ values were measured to be 0.5154 ± 0.0002 (1σ) and 0.5152 ± 0.0003 (1σ). For the 15 °C experiments, λ values were measured to be 0.5110 ± 0.0007 (1σ) and 0.5102 ± 0.0012 (1σ). These

yielded a pooled standard deviation of 0.0005‰ (1σ). The 1σ errors for λ for all of the specific experiments based on the error of the regressions alone ranged from 0.0002 to 0.0012‰. These errors were typically greater than the pooled standard deviation for the replicated experiments. As a result, the reported precision for λ values is the value determined from an individual experiment.

3.3. Results and general trends

Measured values for $^{18}\varepsilon$, λ, and θ are given in Table 1 for each experiment. Isotopic and compositional measurements ($\delta^{18}O$, $\Delta^{17}O$, and $\delta O_2/Ar$) for every time point for each experiment are given in Supplementary Table 1.

Table 1. Measured parameters from *E. coli* respiration experiments.

Carbon source	***E. coli*species**	**O_2reductases**	**T (°C)**	**doubling time (hr)**	**±[a]**	**$^{18}\varepsilon$**	**±[a]**	**λ**	**±[a]**	***θ***	**±[a]**
Acetate	wild type NCM	A family, *bd*-I, *bd*-II	37	2.1	0.4	17.0	0.05	0.5141	0.0009	0.5119	0.0009
Glucose	wild type NCM	A family, *bd*-I, *bd*-II	37	0.7	0.1	17.0	0.1	0.5142	0.0004	0.5120	0.0004
Glycerol	wild type NCM	A family, *bd*-I, *bd*-II	37	1.1	0.2	16.5	0.1	0.5154	0.0002	0.5133	0.0002
Glycerol	wild type NCM	A family, *bd*-I, *bd*-II	37	0.9	0.04	16.4	0.1	0.5152	0.0003	0.5131	0.0003
Glycerol	wild type NCM	A family, *bd*-I, *bd*-II	25	1.4	0.2	15.8	0.1	0.5132	0.0004	0.5113	0.0004
Glycerol	wild type NCM	A family, *bd*-I, *bd*-II	20	3.0	0.1	15.2	0.1	0.5116	0.0007	0.5097	0.0007
Glycerol	wild type NCM	A family, *bd*-I, *bd*-II	17.5	4.3	0.2	14.3	0.1	0.5102	0.0006	0.5084	0.0006
Glycerol	wild type NCM	A family, *bd*-I, *bd*-II	15	6.9	0.6	14.4	0.1	0.5110	0.0007	0.5091	0.0007
Glycerol	wild type NCM	A family, *bd*-I, *bd*-II	15	7.6	0.8	13.9	0.1	0.5102	0.0012	0.5085	0.0012
Glycerol	K-12 CBD1	*bd* -II	37	1.2	0.1	15.0	0.1	0.5147	0.0007	0.5128	0.0007
Glycerol	K-12 MB30	*bd* -I	37	2.6	1.3	15.5	0.2	0.5166	0.0014	0.5146	0.0014
Glycerol	K-12 MB34	A family	37	1.4	0.4	14.9	0.1	0.5115	0.0010	0.5096	0.0010

a. Error bars are 1σ. They are derived from the quality of the fit of the linear regression to data from a specific experiment.

In the experiments, $^{18}\varepsilon$ varied from 13.9 to 17‰, λ varied from 0.510 to 0.515, and θ varied from 0.509 to 0.513. The choice of carbon source (acetate, glucose, or glycerol, had a relatively small impact on these parameters: the carbon source changed $^{18}\varepsilon$ by a maximum of 0.6‰, and both λ and θ by a maximum of 0.001 (Table 1). Note that when carbon sources were varied, the experimental temperature was fixed at 37 °C. From this point on we use θas opposed to λ to discuss mass-law relationships as θ directly describes the relationship between $^{18}\alpha$ and $^{17}\alpha$ (Eq. (4)).

In contrast to the carbon source, the temperature of the experiment (15–37 °C) was related to both the expressed fractionation factor and mass-law slope. In experiments where growth temperature was varied, the relationship between growth temperature and both $^{18}\varepsilon$ and $\theta$was found to be linear (Fig. 4). The data show that $^{18}\varepsilon$ and θ vary as a function of incubation temperature (Fig. 4) as well as growth rate (Fig. 5). This is not surprising given that microbial growth rates typically co-vary positively with temperature (e.g., Ratkowsky et al., 1982) over a limited temperature range. Thus a relationship observed between a parameter and growth temperature will also generally relate to growth rate in closed-system experiments.

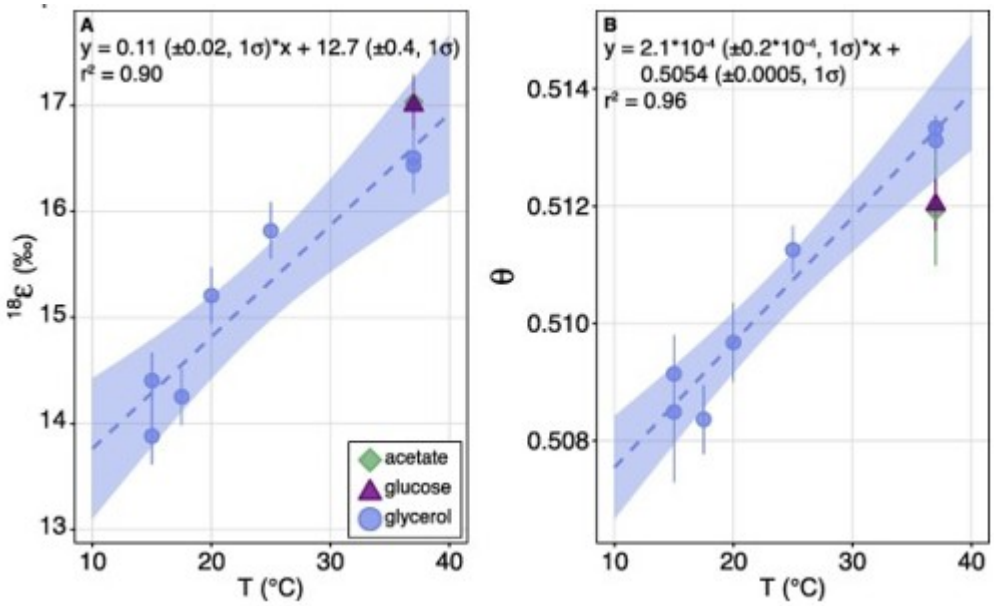

Fig. 4. Relationship between $^{18}\varepsilon$ vs. temperature in (A) and θ vs. temperature in (B). Error bars are 1σ. Fits are only for experiments where glycerol was the carbon source as this was the carbon source used when temperature was varied. We also present the data for wild-type *E. coli* grown on other carbon sources at 37 °C for comparison. The dashed lines are the best-fit lines to the glycerol data with 95% confidence intervals shaded in blue. For $^{18}\varepsilon$, errors are set to 0.26‰, the standard deviation of replicate experiments. For θ, error bars are determined based on the fits for each experiment as these are typically less precise than our observed experimental reproducibility.

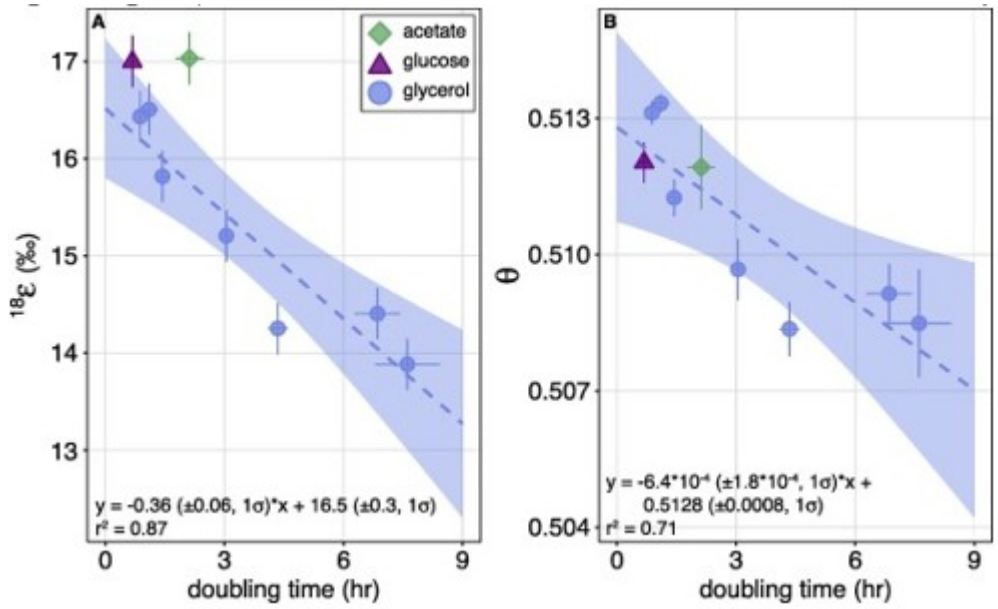

Fig. 5. Relationship between $^{18}\varepsilon$ vs. doubling time in (A) and θ vs. doubling time in (B). Error bars are 1σ. Fits are only for experiments where glycerol was the carbon source as this was the carbon source used when temperature (and thus growth rate) was varied. We also present the data for wild-type *E. coli* grown on other carbon sources at 37 °C for comparison. The dashed lines are the best-fit lines to the glycerol data with 95% confidence intervals shaded in blue. For $^{18}\varepsilon$, errors are set to 0.26‰, the standard deviation of replicate experiments. For θ, error bars are determined based on the fits for each experiment as these are typically less precise than our observed experimental reproducibility. Errors for growth rate are 1σ and are based on exponential fits to the optical density data of each experiment vs. time.

Finally, $^{18}\varepsilon$ and θ were found to positively co-vary (Fig. 6) with higher values of $^{18}\varepsilon$ corresponding to higher θ values.

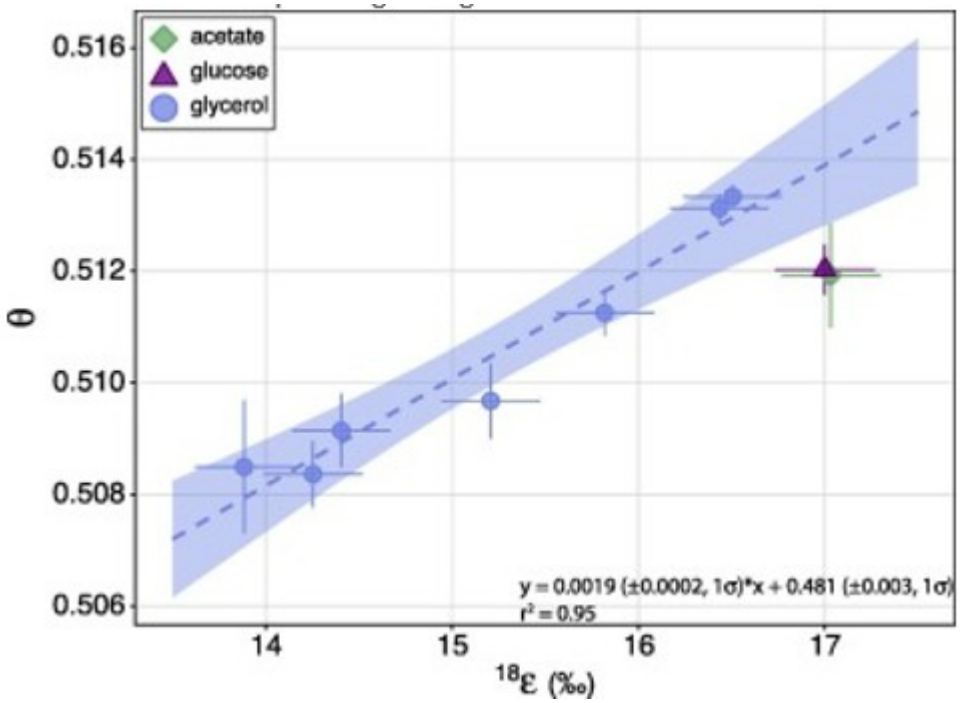

Fig. 6. Relationship between θ and $^{18}\varepsilon$. Fits are only for experiments where glycerol was the carbon source as this was the carbon source used when temperature was varied. We also present the data for wild-type *E. coli* grown on other carbon sources at 37 °C for comparison. The dashed line is the best-fit line to the glycerol data with a 95% confidence interval shaded in blue. For $^{18}\varepsilon$ errors are set to 0.26‰, the standard deviation of replicate experiments. For θ, error bars are determined based on the fits for each experiment as these are typically less precise than our observed experimental reproducibility.

4. Comparison to previous results

4.1. Comparison of $^{18}\varepsilon$ to previous experiments using *E. coli*

Schleser (1979) measured $^{18}\varepsilon$ values for aerobic respiration in *E. coli* K-12 (compared to NCM used here) as a function of temperature from 19 to 36 °C with glucose as the carbon source. A linear fit between $^{18}\varepsilon$ and growth temperature for the Schleser (1979) data yielded a slope of 0.05 (±0.04, 1σ; $r^2 = 0.28$) vs. our slope for the glycerol experiments of 0.11 (±0.02, 1σ; $r^2 = 0.90$; Fig. 7A). Schleser (1979) concluded, that, because of the large fractional error in the slope, the data did not require that $^{18}\varepsilon$ was dependent on temperature. However, at the 2σ level, the slope of Schleser (1979) overlaps with that determined in the experiments presented here.

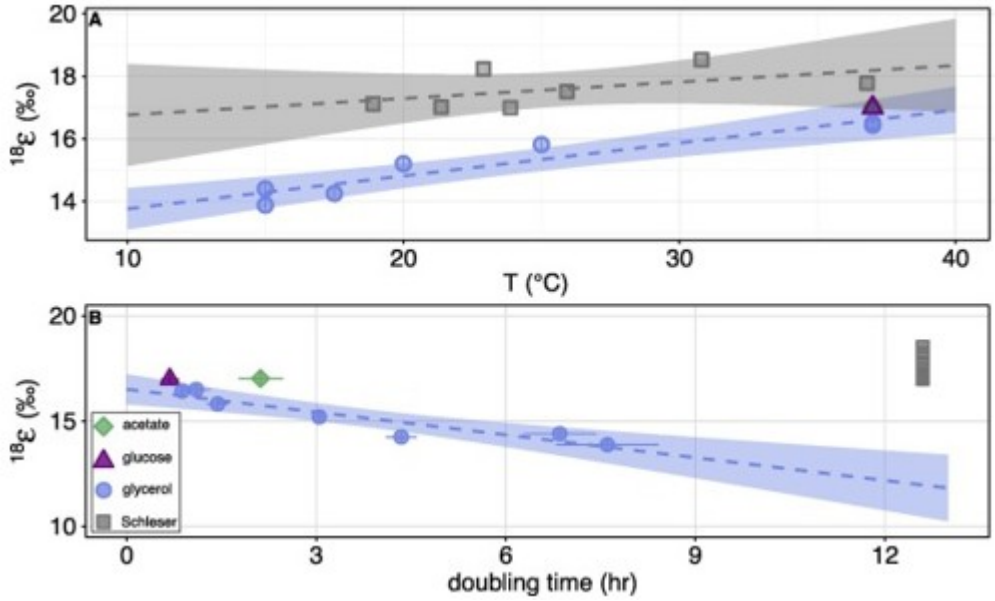

Fig. 7. Comparison of our measurements to those for *E. coli* K-12 given in Schleser (1979). (A) Comparison of $^{18}\varepsilon$ vs. growth temperature. Slopes agree at the 2σ level (see text), but a clear offset between measurements exists. This may be due to use of different *E. coli* strains (K-12 vs. NCM) or methodological differences. (B) Comparison of $^{18}\varepsilon$ vs. growth rate (as doubling time). The dashed lines are the best-fit lines with 95% confidence intervals shaded in blue for our glycerol experiments and grey for the Schleser (1979) experiments. For our determinations of $^{18}\varepsilon$, errors are set to 0.26‰, the standard deviation of replicate experiments. Errors for growth rate are 1σ and are based on exponential fits to the optical density data of each experiment vs. time. Error bars for the Schleser (1979) data are not given as no information on reproducibility is reported.

The $^{18}\varepsilon$ values from Schleser (1979) for *E. coli* range from 17 to 18.5‰ compared to our range of 13.9–17‰. The source of this difference is unclear. One possible explanation is that the magnitudes of respiratory isotope fractionations differ between *E. coli* strains. A second possible explanation is that the temperature dependence is a function of the carbon source used in

the experiment. For example, at 37 °C with *E. coli* NCM grown on glucose, we observed an $^{18}\varepsilon$ value of 17.0‰ while at the same temperature on glucose Schleser (1979)saw an $^{18}\varepsilon$ of 17.8‰ for *E. coli* K-12, which is the closest offset in $^{18}\varepsilon$ at a given temperature between studies.

Other possibilities for the different $^{18}\varepsilon$ values include methodological differences. For example, Schleser (1979) used a chemostat, which allows experiments to be kept at constant cell densities and growth rates while our experiments were done in closed systems with ever increasing numbers of cells. The growth rate for *E. coli* chosen by Schleser (1979)is lower than those used in our experiments. However, as seen in Fig. 7B, the relationship between growth rate and $^{18}\varepsilon$ observed in our experiments (Fig. 5A) does not pass through data of Schleser (1979; Fig. 7B), indicating that differences in growth rate alone are not the explanation. Other methodological differences between closed system growth vs. use of a chemostat could be the cause, but why this would be is unclear. Alternatively, analytical differences between the two studies could be the source of the offset. For example, isotopic measurements were made differently between the two studies: in Schleser (1979) O_2 was converted to CO_2 before analysis while we measured the isotopic composition of O_2 directly. However, whether these analytical differences result in differences for measured $\delta^{18}O$ values is difficult to evaluate as Schleser (1979) did not provide any information on standardization practices (e.g., measurement of air dissolved in water vs. atmospheric air), accuracy of measurements based on standards, or other details that would allow us to directly compare the measurements.

4.2. Comparison to other organisms

Our data is compared to others for microbial cultures (both eukaryotes and bacteria) as well as plants and animals (except humans) for $^{18}\varepsilon$ for aerobic respiration in Fig. 8 and for θ in Fig. 9. To our knowledge, these parameters have never been measured in any archaea. Data from Lane and Dole (1956) are not included in this comparison as measurements made in that study showed poor reproducibility for replicates of the same organism (e.g., 1σ of 6-12‰ for microbial organisms). Previous determinations of $^{18}\varepsilon$ values for bacterial and microbial eukaryotic cultures range from 15.8 to 25.8‰. The values observed here for *E. coli*are 13.9–17.0‰. These are lower on average by a 3–4 per mil compared to previous observations of aerobic respiration and exhibit some of the lowest $^{18}\varepsilon$ values observed for microbial aerobic respiration.

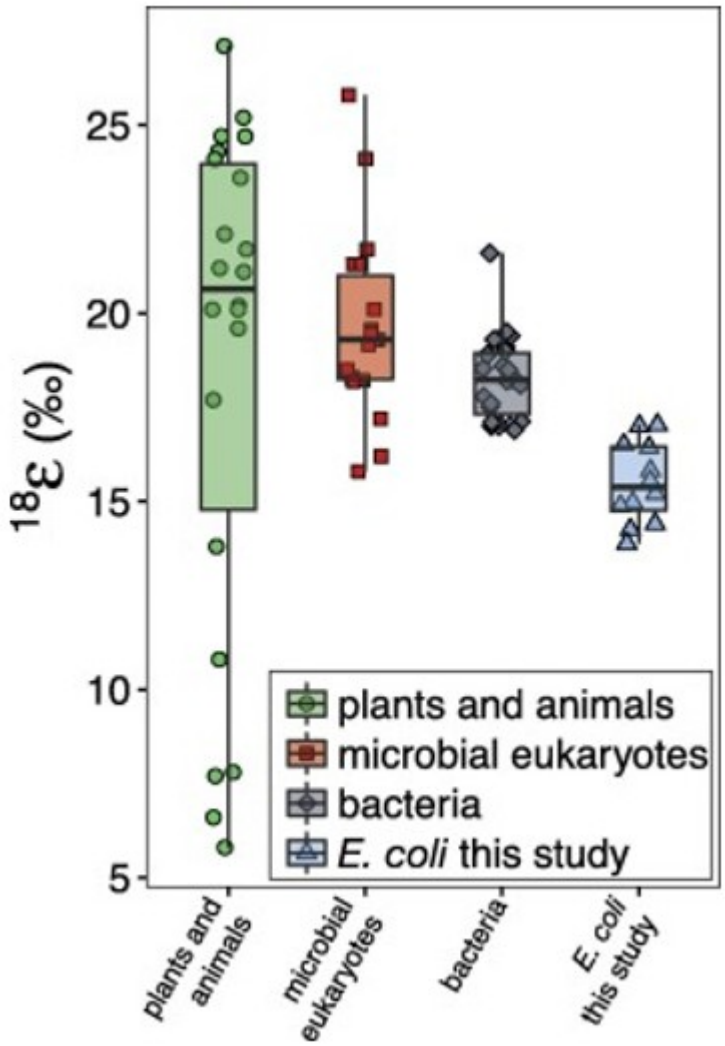

Fig. 8. Measurements of $^{18}\varepsilon$ values for bacterial and eukaryotic microbial cultures and plants and animals, determined in other studies compared to measurements presented here. Boxplots show the mean and 25th to 75th percentiles. Vertical lines show the full data range. Data are from Schleser, 1979, Guy et al., 1989, Robinson et al., 1992, Kiddon et al., 1993, Angert et al., 2003, Barkan and Luz, 2005, and Helman et al. (2005). Only measurements of plants under normal growth conditions are shown—i.e. experiments with various respiratory inhibitors (e.g. cyanide) are not shown. Note, for clarity, the large number (~70) of measurements of $^{18}\varepsilon$ values for human respiration are not shown (Epstein and Zeiri, 1988, Zanconato et al., 1992, Barkan and Luz, 2005). Data from Lane and Dole (1956) are not included, given the poor reproducibility of replicate measurements of microbial experiments (1σ of 6–12‰).

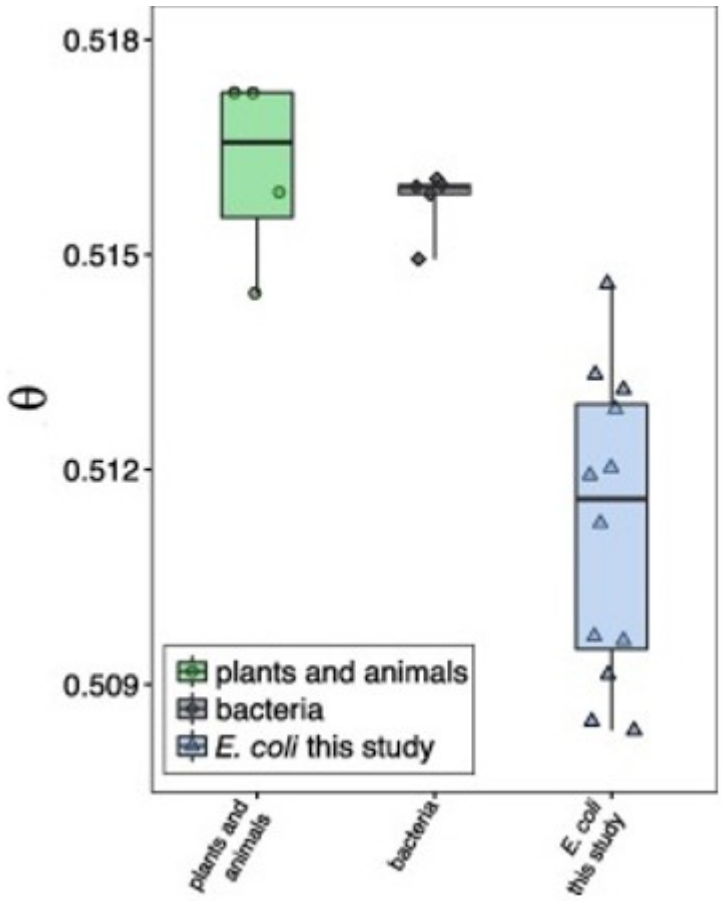

Fig. 9. Measurements of θ values from previous studies of bacterial cultures, eukaryotic microbial cultures, plants, and animals compared to measurements presented here. Boxplots show the mean and 25th to 75th percentiles. Vertical lines show the full data range. Data are from Angert et al., 2003, Barkan and Luz, 2005, and Helman et al. (2005). Only measurements of plants under normal growth conditions are shown—i.e. experiments with various respiratory inhibitors (e.g. cyanide) are not shown.

For θ, the *E. coli* experiments presented here show lower values for aerobic respiration (0.508–0.515) than previously reported for plants, animals, and bacteria (0.515–0.517; Fig. 9). We note that although the θ values we have determined are low compared to other determinations for aerobic respiration, some non-respiratory pathways of O_2 reduction such as photorespiration and reduction of O_2 during phototrophic electron transport yielded even lower θ values of 0.498 and 0.497 respectively (Helman et al., 2005).

5. Controls on the magnitude of $^{18}\varepsilon$ and θ during aerobic respiration in *E. coli*

In contrast to what we observed in our experiments, environmental controls on the magnitudes of $^{18}\varepsilon$ and θ for aerobic respiration are generally not considered except for plants, which have multiple enzymatic pathways for O_2 reduction including heme-copper O_2reductases and the alternative oxidase (and which express different $^{18}\varepsilon$ values; Guy et al., 1989). Rather, microbial systems have generally been thought to express constant oxygen isotope fractionations during aerobic respiration. We evaluated three possibilities for

the cause of the observed variations of $^{18}\varepsilon$ and θ (and their covariaton) in our experiments: (*i*) a direct impact of temperature on respiratory isotope effects; (*ii*) the expression of different respiratory enzymes with varying $^{18}\varepsilon$ and θ values as a function of growth temperature; and (*iii*) changes in the relative rates as a function of experimental temperature of the discrete set of chemical reactions that are associated with the respiration of O_2.

5.1. A direct effect of temperature on respiratory isotope effects

Temperature is known to affect the magnitudes of isotopic fractionations for both equilibrium (Urey, 1947) and kinetic (Bigeleisen and Wolfsberg, 1958) processes. For example, for equilibrium between oxygen isotopes in carbonate vs. water, $^{18}\varepsilon$ [usually given as $1000 \times \ln(^{18}\alpha_{CaCO3\text{-}H2O})$] varies as a function of temperature with a slope of ~0.2–0.25‰/°C at circa room temperatures (e.g., Kim and O'Neil, 1997). This slope is about two times larger in absolute value than that found for *E. coli* during respiration (0.11 ‰/°C; Fig. 4A). Generally, values of $^{18}\varepsilon$ approach 0 ($^{18}\alpha = 1$) as temperatures increase; this is opposite the sense we observed, which suggests that temperature is not directly controlling the magnitude of $^{18}\varepsilon$. However, $^{18}\varepsilon$ does not universally decrease as temperature increases, except as temperatures approach infinity (Stern et al., 1968). Thus we considered that a direct role is possible for temperature in controlling the magnitude of $^{18}\varepsilon$ observed in our experiments.

To test this, we examined the relationship observed between θ and experimental temperature. This relationship is informative because θ is known from both theory and experiments to show a weak dependence on temperature for systems at isotopic equilibrium (Matsuhisa et al., 1978, Cao and Liu, 2011, Dauphas and Schauble, 2016). Whether or not this applies to systems out of isotopic equilibrium and controlled by irreversible reactions (such as during aerobic respiration) is discussed below. For example, theoretical calculations for θ for oxygen-isotope equilibrium between SiO_2 and water, calcite and water, and CO_2 and water all yield increases in θ of less than 0.0008 from 0 to 50 °C (Cao and Liu, 2011). These theoretical calculations are supported by experiments and measurements of environmental samples. For example, θ increases by 0.001 ± 0.001 (1σ) for experimental equilibrations of CO_2 with water from 2 to 37 °C (Hofmann et al., 2012). θ values for isotopic equilibrium between quartz and opal A SiO_2 groups with water are estimated (based on environmental samples) to increase by 0.001 from 0 to 50 °C (Sharp et al., 2016). These results are also consistent with a recently published theoretical analysis of the temperature dependence of θ values for systems at oxygen-isotope equilibrium (Hayles et al., 2018). We note that although Luz and Barkan (2009) observed an increase in θ of 0.019 for O_2dissolved in water equilibrated with air from 3.5 to 25 °C, this was not reproduced by work of Reuer et al. (2007), who observed no change in θ as a function of temperature from 11 to 25 °C. Regardless, for systems at oxygen-isotope equilibrium, it is generally

expected that from 0 to 50 °C, θ will vary by less than 0.001, which is about 5 times less than what we see in our kinetically controlled experiments.

Temperature dependencies of 'intrinsic' kinetic isotope effects (i.e. effects associated with a single, specific chemical reaction) result from similar quantum and statistical mechanical considerations as equilibrium isotope effects (Bigeleisen and Wolfsberg, 1958), and, for oxygen isotopes, the two (kinetic and equilibrium isotope effects) are typically of the same order of magnitude. Consequently, we propose that equilibrium and kinetic isotopic fractionations will lead to similar variations of θ as a function of temperature. If correct, then the shift in θ observed in our experiments is too large, by a factor of at least 5, to be associated with temperature-dependent intrinsic isotope effects during aerobic respiration. Based on this this, we consider a direct control of experimental temperature on the magnitude of the intrinsic isotopic fractionations of a specific chemical reaction to be unlikely and we explore other options below. However, this proposal needs to be confirmed by future work, either experimental or theoretical, on the temperature-dependence of θ for kinetic oxygen-isotope effects.

5.2. Expression of multiple enzymes with different isotopic fractionation factors

Wild-type *E. coli* can synthesize three different respiratory enzymes that reduce O_2 to water: an A-family heme-copper O_2 reductase, and two *bd* O_2 reductases, *bd*-I and *bd*-II respectively. The A-family O_2 reductase is the main terminal O_2 reductase that *E. coli* uses for aerobic respiration under typical laboratory growth conditions (Borisov et al., 2011) with the *bd* O_2 reductases preferentially expressed under low oxygen tensions (typically <10% of air saturation in the growth medium) or stressful growth conditions (e.g., high temperatures) (Rice and Hempfling, 1978, Borisov et al., 2011, Morris and Schmidt, 2013). The isotopic fractionations associated with O_2 reduction for these three enzymes have, to our knowledge, never before been measured. As we did not monitor gene expression in the experiments, it is possible that the genes for the different terminal O_2 reductases were expressed at different experimental temperatures. If correct, and if these terminal O_2 reductases exhibit different $^{18}\varepsilon$ and θ values, then the trend in Fig. 6 could be understood to be a mixing line between the preferential expression of different terminal O_2 reductases as a function of growth temperature.

To test this, we grew *E. coli* K-12 mutants with only one of each of the three terminal O_2reductases, i.e., mutated strains of *E. coli* with the A-family O_2 oxidase only, *bd*-I O_2 oxidase only, and *bd*-II O_2 oxidase only. All were grown at 37 °C with glycerol as the carbon source. Relationships between $^{18}\varepsilon$ vs. θ for these mutants and the wild-type *E. coli* are plotted in Fig. 10. Only the mutant that expresses the A-family heme-copper O_2 reductase falls on the trend defined by the wild-type experiments also grown on glycerol. Both mutants that only express *bd*-type O_2 reductases are off the trend with higher θ values than would be expected based on $^{18}\varepsilon$ values for the wild-type

experiments. Based on the observation that it was only the mutants with the *bd*-type O_2 reductases that did not fall on the expected trend between $^{18}\varepsilon$ and θ, we propose that the changes in $^{18}\varepsilon$ and θ vs. growth temperature are not caused by the differential expression of various terminal O_2 reductases. Additionally, these results indicated that biochemical effects associated with the reduction of O_2 including, for example, substrate channel or binding effects, or modes of electron transfer can give rise to differing values for θ for aerobic respiration depending on the type of O_2 reductase being expressed. Whether or not such differences manifest in nature remains to be tested. Furthermore, these results may indicate that combined measurements of $^{18}\varepsilon$ and θ could be used to probe fundamental aspects of enzymatic reactions, or to help decipher which proteins and pathways are used by different communities to respire O_2 in the environment.

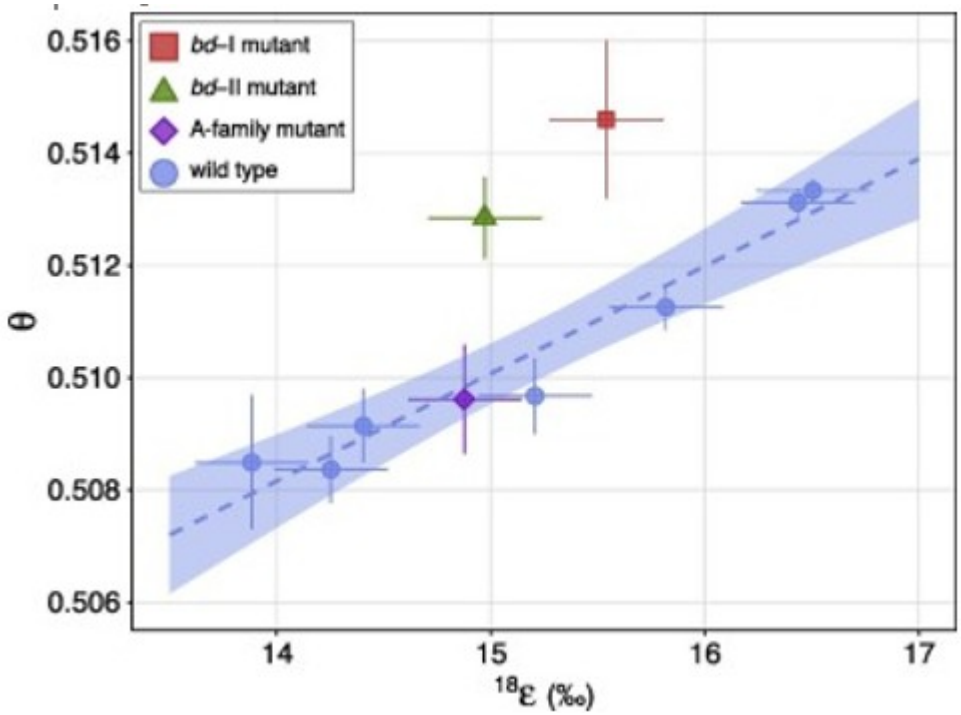

Fig. 10. Comparison of $^{18}\varepsilon$ vs. θ for wild-type *E. coli* grown on glycerol from 15 to 37 °C vs. mutants with only a single terminal O_2 reductase grown on glycerol at 37 °C. The A-family mutant measurement falls on the line defined by the wild-type *E. coli* while the cultures with only *bd*-type mutants do not. We interpret this to indicate that differences in the expression of these O_2 reductases is unlikely to be the cause of the relationship we observed between $^{18}\varepsilon$ vs. θ as a function of growth temperature for wild-type *E. coli*. The dashed line is the best-fit line to the glycerol data with a 95% confidence interval shaded in blue. For $^{18}\varepsilon$, errors are set to 0.26‰, the standard deviation of replicate experiments. For θ, error bars are determined based on the fits for each experiment as these are less precise than our observed experimental reproducibility.

The mutant that only had the A-family heme-copper O_2 reductase exhibited lower values for both $^{18}\varepsilon$ (14.9‰) and θ (0.510) as compared to wild-type *E. coli* grown at 37 °C (16.5 and 0.513 respectively). This difference may result from the mutations causing a disruption in electron flow in *E. coli* and thus modifying expressed isotopic fractionations. Alternatively, the derivation of

mutants from a different wild-type strain of *E. coli* (K-12), compared to the wild-type strain used (NCM) could be the cause.

5.3. Multiple isotopically discriminating steps during O_2 reduction

The consumption of O_2 during aerobic respiration involves, at a minimum, three distinct chemical steps that could affect observed values for isotopic fractionation factors. First, O_2must diffuse to the site of the terminal O_2 reductases (i.e., it must cross cell membranes). Second, the O_2 must transit a hydrophobic channel (Luna et al., 2008) and bind to specific site within an enzyme subunit. Third, while bound, the O_2 must be reduced by four electrons sufficiently rapidly to limit the release of partially reduced reactive-oxygen species (e.g., Naqui et al., 1986). Discussions of isotopic fractionations during aerobic respiration of O_2 by microorganisms in biogeochemical studies generally do not distinguish between these various steps and instead implicitly assign the expression of the isotopic fractionations to the reduction of O_2. This approach requires that the reduction of O_2 be the rate-limiting, isotopically discriminating step.

The presence of multiple isotopically discriminating steps has not been discussed in connection with $^{18}\varepsilon$ and θ values observed for microbial aerobic respiration. However, multiple isotopically discriminating steps/reactions are commonly considered in models and interpretations of isotopic fractionations in other biogeochemical processes. Examples include carbon fixation (e.g., Farquhar et al., 1989); methanogenesis and methanotrophy(e.g., Valentine et al., 2004, Yoshinaga et al., 2014); sulfate reduction (e.g., Rees, 1973, Farquhar et al., 2003); and nitrification (e.g., Buchwald and Casciotti, 2010, Casciotti et al., 2010). To demonstrate the feasibility of these sorts of frameworks to describe our experimental data, we derived a simplified model with two potentially isotopically discriminating steps during O_2 reduction. One step is reversible (i.e. can proceed in both the forward and reverse directions) and the other is irreversible. This simple model shows that the relationship between $^{18}\varepsilon$ and θ is compatible with such a multi-step process.

We assumed that the binding and unbinding of O_2 to the enzyme is reversible. Binding of substrates to enzymes is generally modeled to be a reversible process as described by the Michaelis-Menten formulation of enzyme kinetics (e.g., Johnson and Goody, 2011). We took as the irreversible step the reduction of and breakage of the bond between oxygen atoms in O_2. This involves multiple discrete steps, but the overall process is considered to be irreversible (Wikström, 2006).

These steps can be represented by the following chemical reactions:

(9)O2⇌unbindbindE-O2→reduce2H2O.

Here E-O_2 is the enzyme (E) bound to O_2. We prescribed the $^{18}\alpha$ values of all model steps: binding, unbinding, and bond breakage. We also prescribed $^{17}\alpha$ for all individual steps by choosing a mass law slope θ for each step, which

relates $^{18}\alpha$ to $^{17}\alpha$. In Appendix A.3, we provide a derivation of the model and a description of model assumptions and how the variables in the model are related.

To employ the model, we made the following assumptions. First, we assumed that $^{18}\varepsilon$ for O_2reduction is larger than $^{18}\varepsilon$ for enzymatic binding and unbinding. Our basis is that equilibrium isotope effects for binding of O_2 to heme groups, which occurs during aerobic respiration (Wikström, 2006), vary from ~4 to 6‰ (Tian and Klinman, 1993). This is significantly less than the isotope effect we observed for respiration (~15–17‰) in *E coli*. However, the magnitudes of the kinetic isotope effects associated with enzymatic O_2 binding to O_2reductases are not known.

Second, we assumed that our experiments captured the full reversibility of enzymatic binding such that binding varies from being the rate-limiting step entirely (no reversibility), to equal rates of binding and unbinding (full reversibility). This allowed us to use our experimental results to determine $^{18}\varepsilon$ and θ values of the steps in Eq. (9) (see Appendix A.3for more details). Based on these assumptions, when binding is irreversible (i.e., binding is the rate limiting step), the experimentally measured $^{18}\varepsilon$ value is at a minimum, and equals $^{18}\varepsilon_{bind}$. This minimum occurs in the 15 °C glycerol experiments, the average values of which yield $^{18}\varepsilon_{bind} = 14.1‰$ and $\theta_{bind} = 0.5088$. We further assumed that $^{18}\varepsilon_{unbind} = {}^{18}\varepsilon_{bind}$, and thus, that $\theta_{bind} = \theta_{unbind}$. This is likely incorrect as binding of O_2 to heme groups expresses non-zero equilibrium isotope effects of ~5‰ for hemoglobin and myoglobin (Tian and Klinman, 1993). However, the kinetic isotope effects of binding and unbinding of O_2 to the active site of either of these O_2 reductases (or the A-family heme-copper O_2 reductase of *E. coli*) are not known. Thus, we considered this assumption a useful starting point to limit model complexity. Introduction of non-equal oxygen isotope effects for the binding and unbinding of O_2 simply adds additional free parameters but does not affect any conclusions that follow.

When the binding of O_2 is completely reversible (i.e., rates of binding and unbinding of $O_2$are equal), then based on the assumptions above $^{18}\varepsilon_{measured}$ is at a maximum and equals $^{18}\varepsilon_{reduce}$. Also, these assumptions indicate $\theta_{measured}$ equals θ_{reduce}. Taking the average values from the 37 °C glycerol experiments indicates $^{18}\varepsilon_{reduce} = 16.5‰$ and $\theta_{reduce} = 0.5132$.

With these parameters for the model defined (see Table 2 for a summary), we explored the model's predicted solution space by varying the degree of reversibility of enzymatic binding of O_2. The comparison of the model's predictions vs. the experimental data is given in Fig. 11. As can be seen, the model produces a slightly curved line that largely approximates the trend of the data. Given that we chose the parameters to coincide with the maximum and minimum observed values of $^{18}\alpha$ and θ, the quality of the fit is not surprising. This model can be tested and refined by measuring the equilibrium and kinetic isotope effects associated with binding of O_2 to the different terminal O_2 reductases as has been done with other O_2-binding

enzymes (Tian and Klinman, 1993). The model also predicts that the rates of binding and unbinding are of a similar magnitude as the reduction rates of O_2 and that one of these rates varies as a function of growth temperature, which provides another testable prediction.

Table 2. Values used in the respiration model.

Step	**$^{18}\varepsilon$ (‰)**	***θ***
Bind	14.1	0.5088
Unbind	14.1	0.5088
Reduce	16.5	0.5132

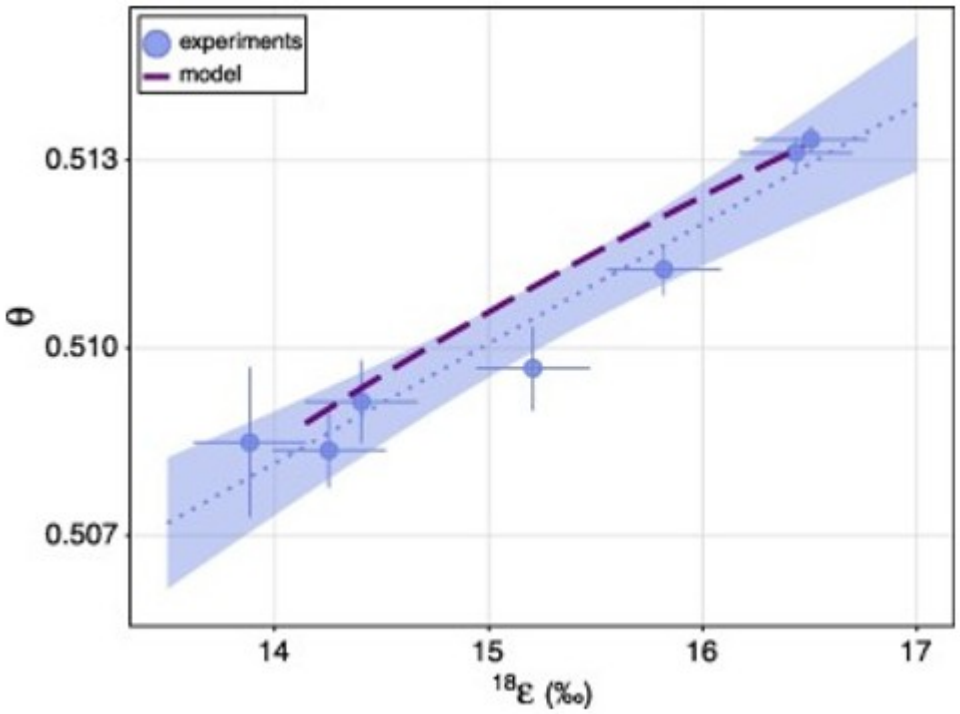

Fig. 11. Comparison of measured values of $^{18}\varepsilon$ and θ for experiments with wild-type *E. coli* grown on glycerol vs. a model of respiration that includes multiple isotopically discriminating steps (see Section 5.3). The blue dotted line is the best-fit linear regression to the experimental data and the blue shading represents the 95% confidence interval on that fit. Error bars are 1σ. For $^{18}\varepsilon$, errors are set to 0.26‰, the standard deviation of replicate experiments. For θ, error bars are determined based on the fits for each experiment as these are less precise than our observed experimental reproducibility.

The key point is that the experimental data is consistent with a simple, isotopically enabled model of aerobic respiration. Consequently, we propose that temperature (or growth rate) could change the relative rates of enzyme binding vs. reduction, and that this provides a plausible explanation for the data.

6. Implications for the biogeochemical cycling of O_2

Measurements of the isotopic composition of O_2 dissolved in marine waters are generally considered in the context of respiration coupled with advective and diffusional processes that mix water masses along or across isopycnal surfaces (Kroopnick and Craig, 1976, Bender, 1990, Levine et al., 2009, Nicholson et al., 2014). A common conclusion of such studies (e.g., Kroopnick and Craig, 1976, Bender, 1990, Levine et al., 2009) is that it is challenging to reproduce the observed relationship between the concentration and $\delta^{18}O$ value of dissolved O_2 in the ocean using typical $^{18}\varepsilon$ values of ~18‰ unless one invokes the presence of low-O_2 water masses with $\delta^{18}O$ values of dissolved O_2 elevated by tens of per mil relative to the maximum values observed in nature (see Section 1.2). To illustrate how our results can help inform this issue, we applied our measured fractionation factors to the one dimensional advection-reaction-diffusion equation for O_2 transport and respiration in the oceans given by Levine et al. (2009):

(10)∂[O2]∂t=K∂2[O2]∂x2-u∂[O2]∂x-J.

In Eq. (11), K is the eddy diffusivity, u is the advective velocity, and J is the respiration rate.

The respiration rates (J) of $^{16}O^{18}O$ and $^{16}O^{17}O$ are related to the respiration rate of $^{16}O_2$ as follows (Levine et al., 2009):

(11)J16O18O=J16O2×18α×[16O18O][16O2]

and

(12)J16O17O=J16O2×18αθ×[16O17O][16O2]

where brackets denote concentrations. We solved these equations using Matlab's partial differential equation solver "pdepe". We used a value for K of 1000 m^2/s and for u of 0.0004 m/s, which are the baseline values given in Levine et al. (2009). The sensitivity of $\delta^{18}O$ values of dissolved O_2 in the ocean to these values is discussed in detail in Levine et al. (2009). We used a path length of 5000 km for the one-dimensional flow. Following Levine et al. (2009), we set the boundary condition at the start of the flow to be in equilibrium with the atmosphere (300 µmoles O_2 per kg seawater), while the end of the flow was set as a no-flux wall. We chose the J term to be 1.287 µmol/kg/yr such that the lowest concentration of O_2 (which occurs at the end of the path at 5000 km) is 3% of saturation—this marks the lowest observed value in the oceans for which measurements of the $\delta^{18}O$ value of dissolved O_2 have been made.

As discussed, a typical $^{18}\varepsilon$ value used to model microbial respiration in the ocean is 18‰ (e.g., Levine et al., 2009) and we adopted this as the reference value for comparison to $^{18}\varepsilon$ values derived from our *E. coli* experiments. We used the observed temperature dependence of $^{18}\varepsilon$ in *E. coli* to estimate an $^{18}\varepsilon$ the for ocean interior based on our experiments. Most marine respiration in the oceans below the mixed layer occurs in the top 1200 m at an average temperature of 7.4 °C (Sarmiento and Gruber, 2006).

Using 7.4 °C as the temperature of respiration and the experimentally observed relationship between $^{18}\varepsilon$ vs. temperature of *E. coli* (Fig. 4A) yielded an $^{18}\varepsilon$ value of 13.5‰.

In Fig. 12, we provide the modeled results using these two different $^{18}\varepsilon$ values to measurements of the $\delta^{18}O$ values of marine dissolved O_2 from a variety of studies (Kroopnick and Craig, 1976, Kroopnick, 1987, Quay et al., 1993, Hendricks et al., 2005, Nakayama et al., 2007, Levine et al., 2009). We assumed that the initial O_2 concentration was the saturation concentration. From 100 to 50% of O_2 saturation, observed $\delta^{18}O$ of O_2values were simulated with equal visual fidelity given either choice of $^{18}\varepsilon$. From 50 to 25% of saturation, the $^{18}\varepsilon$ value constrained by our experiments (13.5‰) predicted $\delta^{18}O$ values consistent with the data. In contrast, an $^{18}\varepsilon$ value of 18‰ overpredicted the $\delta^{18}O$ value of dissolved O_2 from 50 to 25% of saturation. At saturations less than 10%, both curves overpredicted the $\delta^{18}O$ value of dissolved O_2 relative to observations. The choice of $^{18}\varepsilon$ of 18‰ predicted, at 3% of saturation, the $\delta^{18}O$ value of O_2 should be 38.9‰. This is significantly larger than the maximum value observed in the oceans of 21.6‰. In contrast, the use of the $^{18}\varepsilon$ value of 13.5‰ calibrated by the *E. coli* experiments predicted a $\delta^{18}O$ of O_2 in the dark ocean at 3% saturation of 29.2‰. This value is also higher than the maximum measured $\delta^{18}O$ value for O_2 in the ocean; however it is closer to observed values seen in natural samples than if we had assumed a respiratory $^{18}\varepsilon$ of 18‰. As such, we propose that oceanic data are qualitatively consistent with our experimental data such that at colder temperatures (as in dark ocean waters), $^{18}\varepsilon$ values are lower than observed at warmer temperatures (as in surface waters outside of the high latitudes).

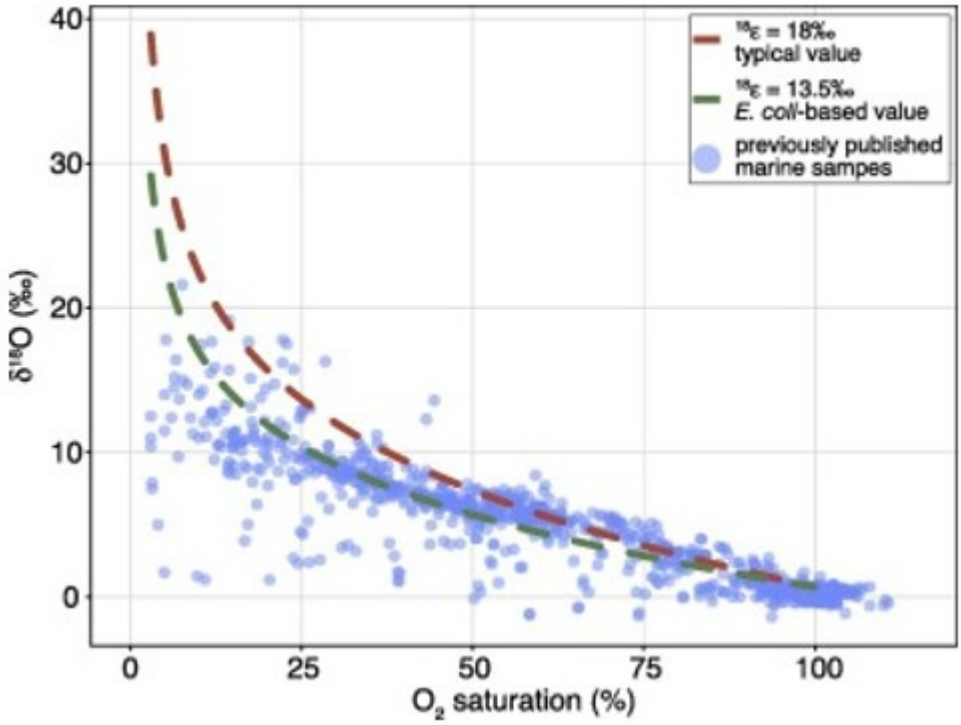

Fig. 12. $\delta^{18}O$ values of O_2 dissolved in the ocean vs. % O_2 saturation. The red curve shows model-predicted values for the typically assumed $^{18}\varepsilon$ value of 18‰. The green curve shows the relationship predicted assuming a respiratory isotope effect of 13.5‰ for the ocean (50–1200 m) based on the relationship between $^{18}\varepsilon$ and temperature observed in our experiments, and assuming 7.4 °C for average ocean temperature between 50 and 1200 m (see main text). We assume that at 100% saturation $\delta^{18}O$ of dissolved O_2 in the surface ocean is 0.7‰, the approximate value for equilibrium between atmospheric and dissolved O_2 in seawater (Kroopnick and Craig, 1972, Benson and Krause, 1984). Data are from Kroopnick and Craig, 1976, Kroopnick, 1987, Quay et al., 1993, Hendricks et al., 2005, Nakayama et al., 2007, and Levine et al. (2009).

Additional support for the dependence of $^{18}\varepsilon$ on temperature from natural systems comes from water column measurements (0–400 m depths) of the concentration and $\delta^{18}O$ value of dissolved O_2 from the Estuary and Gulf of St. Lawrence (Lehmann et al., 2009). When the data in that study was analyzed in the context of Rayleigh fractionation process, the $^{18}\varepsilon$ was found to be 10.8‰ for respiration in the water column. Given that this number is much less than the value typically assumed for respiration (18–22‰), the authors concluded that significant amounts of respiration must be occurring in the sediments where diffusive processes reduced the expressed $^{18}\varepsilon$ values of respiration. Interestingly, temperatures below the mixed layer vary from ~0 to 5 °C in this region (e.g., Savenkoff et al., 1996). Based on the relationship between temperature and $^{18}\varepsilon$ derived from the *E. coli* experiments, for the temperature range of 0–5 °C, our experiments would predict $^{18}\varepsilon$ values for aerobic respiration from 12.7 to 13.2‰. These values are similar to the $^{18}\varepsilon$ observed in the Estuary and Gulf of St. Lawrence (10.8‰). Consequently, this system provides additional support for our hypothesis that gradients in environmental temperatures can cause changes in the expressed $^{18}\varepsilon$ values

of aerobic microbes and leave a measureable imprint in the $\delta^{18}O$ values of residual seawater O_2.

$^{18}\varepsilon$ values have been estimated for the surface ocean mixed layer in high latitude regions using models based on estimates of rates of photosynthesis, respiration, and gas exchangebetween the atmosphere and oceans. For the subarctic Pacific, 11–12 °C mixed layer waters were calculated to have an $^{18}\varepsilon$ for respiration of 20–25‰ (Quay et al., 1993)—values significantly above what the *E. coli* experiments would predict at these temperatures (~14‰). Similarly, in the Southern Ocean, models of respiration in mixed layer waters at temperatures of 0–12 °C yielded an average $^{18}\varepsilon$ value of 22‰ with no clear dependence on temperature (Hendricks et al., 2004). Again this estimate is significantly above what the *E. coli* data would predict (12.7–14‰). Importantly, when Quay et al. (1993) examined thermocline waters with an average temperature of ~8 °C in the subarctic Pacific (in the same location as where the mixed-layer waters were sampled), they calculated an $^{18}\varepsilon$ of 12 ± 2‰. This is similar to an estimate based on our *E. coli* experiments of 13.6‰. Such a comparison cannot be made for the Southern Ocean data of Hendricks et al. (2004) as only mixed layer waters were measured. Quay et al. (1993) proposed that one possible cause of the calculated difference between the estimated $^{18}\varepsilon$ values for mixed-layer and thermocline waters was that the population of organisms in the mixed layer and thermocline exhibit different $^{18}\varepsilon$ values. This is plausible as the mixed layer hosts higher active proportions of autotrophic organisms than occurs in deeper waters, which in turn tend to contain higher proportions of heterotrophic bacteria Given that *E. coli* is a model heterotrophic bacterium, our results are consistent with this idea. Thus our results are likely most relevant to natural systems where respiration is dominated by heterotrophic bacteria (as occurs below the mixed layer and in the sediments). Further experiments on the effects of temperature on respiratory $^{18}\varepsilon$ values of Cyanobacteria and algae could test this idea—though we note that these organisms also employ similar versions of respiratory machinery in their mitochondrial electron transport chains (e.g. A-family heme-copper O_2 oxidases). Regardless, our results are consistent with observed $^{18}\varepsilon$ values derived for the cold, deep oceans where heterotrophic bacteria are the main consumers of O_2.

Now we turn to the implications of the model for $\Delta^{17}O$ data. Comparison of the model to data requires a dataset showing substantial changes in O_2 concentration. We are aware of only one dataset with $\Delta^{17}O$ values measured on dissolved O_2 with substantial depletions (>25%) in O_2 concentrations relative to saturation. That is from Hendricks et al. (2005) for the equatorial Pacific at depths from 0 to 300 m. Interpreting this data set is not simple in that waters sampled likely had complicated histories of photosynthesis and respiration as a function of time. For example, some waters likely spent time at deeper depths before returning to the euphotic zone.

The average temperature of respiration from this study was 17 °C for samples with <75% saturation. At 17 °C, the *E. coli* experiments predict θ to be 0.5090 (based on the relationship in Fig. 4B) and $^{18}\varepsilon$ to be 14.5‰ (based on the relationship give in Fig. 4A). The typical λ value used to describe respiration in the oceans is 0.518. This value of λ combined with an $^{18}\varepsilon$ value of 18‰ yields a value for θ of 0.5157 based on equation (8). These two values for θ were used in the model and then compared to environmental data.

We only compared the model to data with O_2 concentrations less than 75% of saturation because photosynthesis after subduction below the mixed layer is probably small in most of these samples. Many samples with higher O_2 saturation (>75%) are influenced by co-occurring photosynthesis and respiration. Specifically, as O_2 concentrations decline from 100 to 75% of saturation in the Hendricks et al. (2005) dataset, $\Delta^{17}O$ values increase (Fig. 13). Such increases are caused by the addition of photosynthetically derived O_2 to a water mass (Luz and Barkan, 2000, Hendricks et al., 2005). Waters at 75% O_2 saturation have an average $\Delta^{17}O$ value of 0.104‰ in the Hendricks et al. (2005) dataset (taken as the average $\Delta^{17}O$ value of waters from 65 to 85% saturation). We used this number (0.104‰) as the initial $\Delta^{17}O$ value, and model the subsequent changes in $\Delta^{17}O$ due to respiration and mixing between water masses for water masses with less than 75% O_2 saturation.

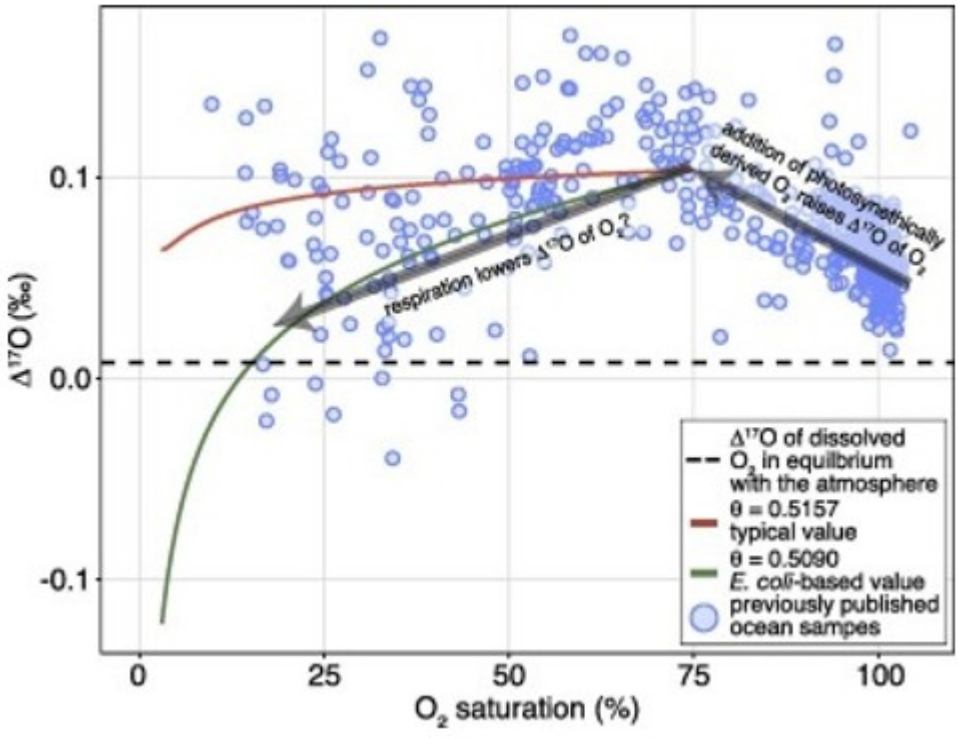

Fig. 13. $\Delta^{17}O$ values of O_2 dissolved in the equatorial Pacific Ocean vs. model-predicted values for a typically assumed θ value (0.5157: red line) vs. that (0.5090: green line) for the depth interval of 50–1200 m (average ocean temperature = 7.4 °C), based on the relationship between θ and experimental

temperature observed in our experiments (green line). Data are from 0 to 300 m depth (Hendricks et al., 2005).

We compared the model calculations using the two θ values (0.5090 and 0.5157) to the Hendricks et al. (2005) dataset in Fig. 13. These are the values for θ for respiration at 17 °C (the average temperature of water masses from which the data was derived) and the typically assumed value for θ (see above). As discussed, it is commonly thought that respiration has only a marginal effect on $\Delta^{17}O$, and only at low O_2 concentrations when non-linear mixing effects become significant. When we ran our model with the 'typical' θ value of previous studies (0.5157), we simulated a marginal decrease in $\Delta^{17}O$ of only 0.012‰ from 75 to 25% O_2 saturation (Fig. 13) consistent with typical expectations. This model failed to capture the general decline of $\Delta^{17}O$ vs. O_2 concentration seen in the Hendricks et al. (2005)dataset (Fig. 13). The use of the θ value determined based on the *E. coli* experiments in the model predicted a decrease in $\Delta^{17}O$ of 0.066‰ as respiration reduces dissolved O_2saturations from 75 to 25% and simulated negative $\Delta^{17}O$ values for O_2 concentrations less than ~15% of saturation. The negative $\Delta^{17}O$ values result from two processes: First, they largely result from the lower θ value used for respiration here relative to the reference value in the definition of $\Delta^{17}O$. Second, they also result from the effects of mixing (due to diffusion) of water masses with differing $\delta^{18}O$ values (Nicholson et al., 2014). This second effect is observed in both model runs as O_2 concentrations decline, but as can be seen in Fig. 13when the typical θ is used, this effect is insufficient to generate negative $\Delta^{17}O$ values. The decline in $\Delta^{17}O$ predicted by our model captures the general decrease in $\Delta^{17}O$ vs. O_2concentration for samples below ~75% of O_2 saturation (Fig. 13). For example, the average decrease in $\Delta^{17}O$ below 75% saturation in the Hendricks et al. (2005) data is 0.0010‰/%saturation. The model using the θ derived from the *E. coli* experiments predicted a slope of 0.0017‰/%saturation from 75 to 10% of saturation (i.e., the concentration range of the Hendricks et al. (2005) data). If we restrict the model to 75–25% saturation (which reduces the curvature of the model), the model slope is 0.0013‰/% saturation, and thus similar to the observed slope in the data. However, the model clearly does not capture the full range of $\Delta^{17}O$ observed in the Equatorial East Pacific—other causes for these variations are given in Hendricks et al. (2005). Regardless, the key point is that using a lower-than-typical value for θ based on constraints from our experiments in a simple biogeochemical model of respiration is consistent with environmental data. These lower θ values also allow for respiration below the mixed layer to generate negative $\Delta^{17}O$ values at O_2 concentrations as is seen in nature. If correct, such changes in θ will manifest themselves as function of both the temperature, amount of respiration, and amount of mixing between water masses. Consideration of such could be important for understanding the meaning of $\Delta^{17}O$ values, and especially negative $\Delta^{17}O$ values, of dissolved O_2 in cold water masses in the ocean below the mixed layer.

7. Summary

We demonstrated that during closed-system growth of *E. coli*, experimental conditions such as temperature and/or growth rate influence the expressed isotopic fractionations for aerobic respiration. Varying the carbon source between glycerol, acetate, and glucose yielded minor changes in isotopic fractionations with $^{18}\varepsilon$ varying by <0.6‰ and $\theta < 0.001$. On the other hand, decreasing growth temperature from 37 to 15 °C caused $^{18}\varepsilon$ to decrease by ~2.5‰ and θ to decrease by 0.005.

We interpreted this change to result from variations in the rate of binding vs. unbinding of $O_2$to the enzyme relative to the rate of reduction as a function of growth temperature. Using a simple isotope mass-balance model of fractionations during O_2 respiration, we demonstrated that this mechanism provides a plausible explanation for variations in $^{18}\varepsilon$ and θ that we observed. This explanation requires that binding rates of O_2 to the enzyme change, as a function of temperature (and/or growth rate), relative to O_2 reduction rates during aerobic respiration in *E. coli*. In addition, binding rates, unbinding rates, and O_2 reduction rates must be of similar magnitude. Finally, we observed that θ varies by 0.005 depending on which O_2reductase is used by *E. coli* during aerobic respiration. These results suggest that the mechanism of how enzymes bind and/or reduce O_2 during aerobic respiration can cause variations in θ.

We placed these results into a biogeochemical framework through the use of a 1-D advection-reaction-diffusion equation. We used this model to calculate and compare how both $\delta^{18}O$ and $\Delta^{17}O$ values of dissolved O_2 vary as a function of the amount of consumed using both the generally assumed values $^{18}\alpha$ and θ for aerobic respiration and those determined by the experiments for respiration in the ocean below the mixed layer. We compared the predictions of our model to environmental data. We found that model results predicted using $^{18}\varepsilon$ and θ values determined from the *E. coli* measurements were better able to explain trends in $\delta^{18}O$ and $\Delta^{17}O$ of dissolved O_2 vs. the concentration of dissolved O_2(relative to the starting value) compared to the use of typical $^{18}\varepsilon$ and θ. Based on this, we proposed that our observation that values of $^{18}\varepsilon$ and θ for aerobic respiration that are lower in colder experiments can be successfully applied to the environment. Specifically our experimental results provide an explanation for the lower observed $^{18}\varepsilon$ values calculated from $\delta^{18}O$ values and concentration measurements of O_2 in below the mixed layer (e.g., in the deep ocean). Additionally, the lower values of θ observed at colder experimental temperatures provides an explanation for the observation that $\Delta^{17}O$ values of O_2 dissolved in seawater may be less than 0‰.

Going forward, it will be key to demonstrate on natural communities whether the insights gained from these experiments in a model microbial system are characteristic of those aerobic communities found in natural systems. More observations of $\Delta^{17}O$ in cold-water systems in the oceans (both from the

surface and at depth), would help elucidate this. Additionally, experiments on photosynthetic bacteria and eukaryotes and obligately heterotrophic eukaryotes where growth parameters are varied would be useful as well as incubations of natural planktonic communities from a variety of thermal settings (e.g., Arctic vs. equatorial surface waters). Regardless, this study offers an experimentally based explanation for the difference between predicted values of $\delta^{18}O$ and $\Delta^{17}O$ of O_2 in the deep oceans vs. in shallow waters.

Acknowledgments

DAS acknowledges funding from a NOAA C&GC postdoctoral fellowship. WWF acknowledges support from the David and Lucile Packard Foundation. We thank J Hemp for providing *E. coli* mutant strains, and S Kopf for providing us with *E. coli* NCM and the trace-metal solution. We thank D Sigman, S Kopf, and F Morel for helpful discussions.

Appendix A.

A.1. Mass spectrometry details

Between 20–40 μmoles of total O_2 and Ar were introduced into the bellows of the mass spectrometer for both the sample and standard. The standard used is a mixture of O_2 (96%) and Ar (4%) purchased from BOC Gases. This standard has a similar molecular and isotopic composition as air. Relative to air, its $\delta^{18}O$ value is 0.716‰ (±0.004, 1 standard error [s.e.]); its $\Delta^{17}O$ value is −0.025‰ (±0.001, 1 s.e.); and its $\delta O_2/Ar$ value is -8.8‰ (±0.1, 1 s.e.).

Samples were measured with a current of ~5.5 nA on mass 32 (5.5 V registered on the Faraday cup with a 10^9 Ω gain amplifier). Samples were run in measurement blocks consisting of 24 sample-standard bracketing cycles with 8 second idle times between each measurement of the sample or standard. Signals were integrated for 16 seconds and 6 blocks of cycles were measured (2304 s of integration). Internal precisions for a complete analysis (i.e. standard deviations [1σ] for all cycles across all measurement blocks of a single sample) for $\delta^{18}O$ and $\Delta^{17}O$ measurements were generally <0.005‰ and 0.005–0.01‰ respectively. These were similar to those expected based on counting statistics (0.002 and 0.005‰). Following each $\delta^{18}O$ and $\Delta^{17}O$ measurement block, the signal for mass 28 ($^{28}N_2$), 32 ($^{32}O_2$), and 40 (^{40}Ar) were measured via a ‘peak-hopping’ algorithm. Typical internal precision for $\delta O_2/Ar$ was <0.2‰. $\delta^{18}O$ and $\Delta^{17}O$ were corrected for ionization effects associated with differences in $\delta O_2/Ar$ following the method outlined by Barkan and Luz (2003). All samples were normalized to aliquots of air purified, transferred, and measured in identical fashion. $\delta O_2/Ar$ and $\delta^{18}O$ values of samples originally dissolved in water were corrected for dissolution of some gas in the water removed from the sampling flask following Luz et al. (2002).

External precision of the analyses was monitored via measurement of air samples collected at Princeton (sampled in the laboratory) and gases derived

from $HgCl_2$-poisoned deionized water equilibrated with the atmosphere. Measurements of both were made over the course of 10 months and span the entire time experimental samples were measured. Air samples were introduced directly into the automatic purification line described above. The external precision (1σ) of air samples ($n = 32$) for $\delta^{18}O$, $\Delta^{17}O$, and $\delta O_2/Ar$ were 0.025, 0.007, and, 0.74‰ respectively. Poisoned, deionized water samples were treated identically as samples as described above. External precision (1σ) of poisoned deionized water ($n = 14$) for $\delta^{18}O$, $\Delta^{17}O$, and $\delta O_2/Ar$ were 0.050, 0.008, and 0.8‰ respectively.

Accuracy of measurements was established by experimentally equilibrating gas dissolved in deionized water and comparing determinations of $\delta O_2/Ar$, $\delta^{18}O$, and $\Delta^{17}O$ made here against previous determinations of these values. Air samples cannot be used for this purpose as all samples are normalized to air samples measured in the lab. $\delta O_2/Ar$ values for $HgCl_2$-poisoned deionized waters (the temperature of the lab varies between 20 and 25 °C) were -89.3 ± 0.3‰ (1 standard error [s.e.], $n = 14$). Based on measurements of the O_2/Ar ratio in the atmosphere (Glueckauf, 1951) and gas solubilities (Garcia and Gordon, 1992), the expected value for $\delta O_2/Ar$ of gas dissolved in deionized water should range between −90.0 and −90.8‰. These values carry an associated error of ~±1‰ based on uncertainties in the O_2/Ar ratio of the atmosphere and the solubility equations. Similar results are obtained if Bunsen coefficients are used (Weiss, 1970). Based on Bunsen coefficients the $\delta O_2/Ar$ value of gas dissolved in deionized water should be between −90.1 and −90.5‰ over this temperature range with an associated error of ±4‰. Thus our determination for the δO/Ar value for air dissolved in deionized water is within uncertainty of the expected value and we consider it accurate. A different determination of the $\delta O_2/Ar$ value of air dissolved in deionized water (at 25 °C) by Barkan and Luz (2003) determined the $\delta O_2/Ar$ of gas dissolved in deionized water at 25 °C to be −88.8 ± 0.1‰ (1σ). They used methods similar to ours and considered their determination to be accurate.

Our average measured $\delta^{18}O$ value for O_2 dissolved in deionized water was 0.666 ± 0.014‰ (1 s.e., $n = 14$). Previous determinations of this between 20 and 25 °C range from 0.637 to 0.722‰ (Keedakkadan and Abe, 2015). Our value is intermediate to these and is similar to previous determinations made at Princeton on seawater at 25 °C (0.640 ± 0.16‰, 1 s.e.; Reuer et al., 2007). Thus we consider our $\delta^{18}O_{air}$ determinations to be accurate.

The average $\Delta^{17}O_{air}$ value of air dissolved in 20–25 °C deionized water from our experiments was 0.000 ± 0.002 (1 s.e. $n = 14$). Previous determinations of this value have ranged from 0.005 to 0.018‰ (Keedakkadan and Abe, 2015) and are higher by ~ 0.01‰ on average than ours. We explored the cause of the lower-than-expected $\Delta^{17}O$ for air dissolved in deionized water relative to air as follows.

First, we examined whether our use of molecular sieves to transfer samples from our purification line to the mass spectrometer was introducing analytical effects. To do this, we froze our working O_2:Ar gas standard (to which all samples are compared) onto the molecular sieves. We then released the gas into the mass spectrometer and compared it to an aliquot of the same standard released directly to the mass spectrometer without interaction with the molecular sieves. $\Delta^{17}O$ values were unfractionated, or nearly so, ($\Delta^{17}O = -0.002$‰ sieve vs. no sieve, ±0.001‰, 1 s.e.). Thus, use of the molecular sieves does not have a noticeable effect on $\Delta^{17}O$ values.

Second, we tested for a dependence of $\Delta^{17}O$ on total sample size. This was done by equilibrating water with air and admitting 200–300 ml aliquots of this water into pre-evacuated, pre-poisoned 500 ml flasks. The pressure of gas extracted from these liquids varied between 22–35 mbar (±50% relative) in the mass spectrometer bellows at full expansion. On a plot of $\Delta^{17}O$ vs. O_2 sample size, the slope and intercept are both within error of zero at the 2σ level (Fig. A1). Based on this, we believe our determinations of $\Delta^{17}O$ are reproducible and unaffected by sample size or use of the molecular sieves. We expect that our difference in $\Delta^{17}O$ for air vs. air dissolved in water may be related to the different protocols involved in extracting gas dissolved in liquid vs. measuring atmospheric samples. For example, we found that fractionations for $\delta^{18}O$ and $\Delta^{17}O$ could be introduced by modulating the temperature flasks were immersed in before introduction of gas to the purification line and by modifying gas transfer times (Fig. A2). Regardless, as our determination of values for $^{18}\alpha$ and λ are based on the comparison of isotopic compositions of dissolved gases measured only in our laboratory, and for a finite time period, any constant offset in $\Delta^{17}O$ relative to O_2 in air is unimportant.

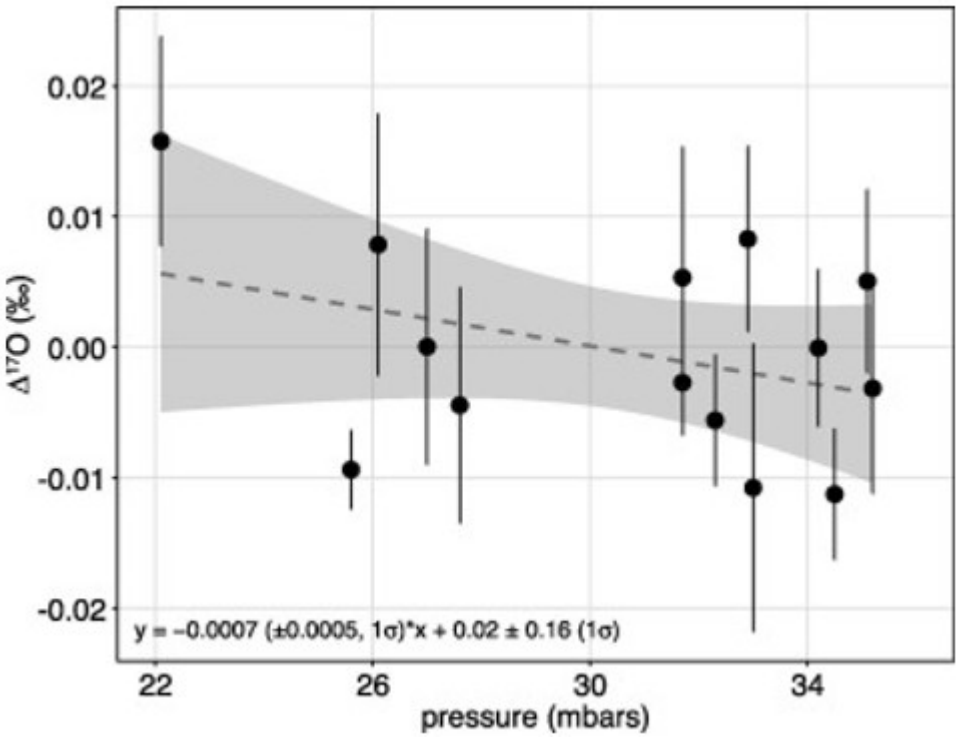

Fig. A1. Dependence of $\Delta^{17}O$ of O_2 dissolved in 20–25 °C deionized water (poisoned with $HgCl_2$) on the sample size (measured as the pressure of the sample in the mass spectrometer bellows at full extension). The gray dotted line is the best-fit linear regression to the experimental data and the gray shading represents the 95% confidence interval on that fit. Neither the slope nor the intercept was distinguishable from 0 (at the 2σ level). Error bars are 1σ.

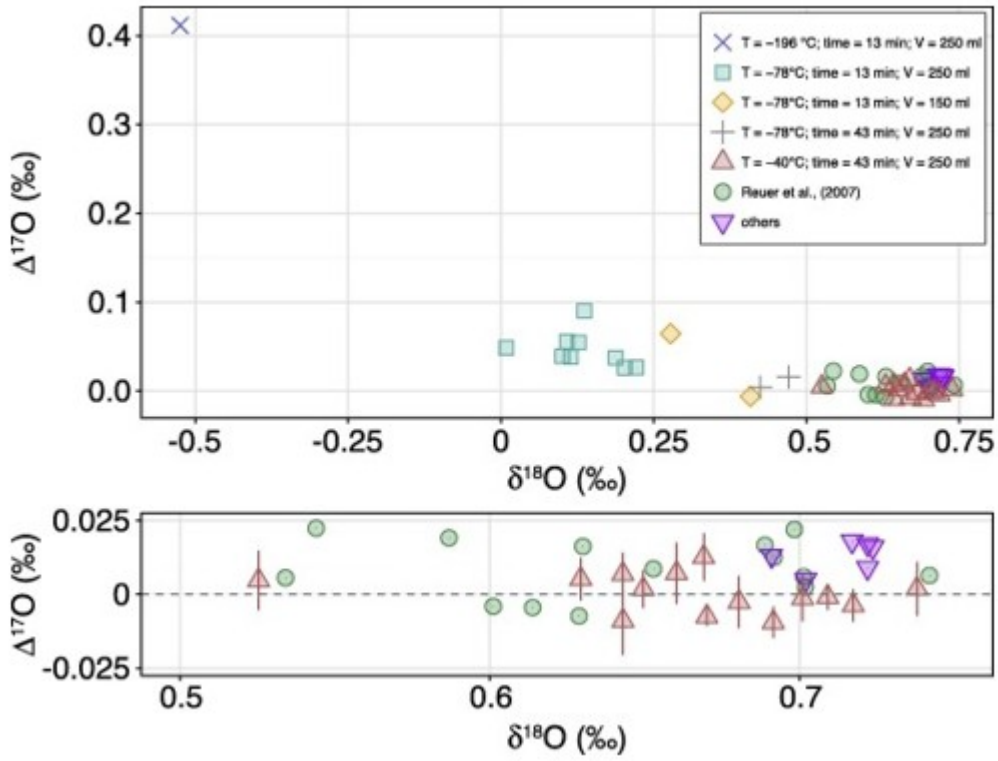

Fig. A2. Relationship between $\delta^{18}O$ and $\Delta^{17}O$ of O_2 dissolved in deionized, poisoned water in equilibrium with the atmosphere. “T” is the temperature the flask was cooled to before transfer; “time” refers to the transfer time of the gas to the first molecular sieve trap; “V” is the volume of water in the flask. We note that freezing residual water in flasks before introduction of gas to the purification line at different temperatures or transferring for different times resulted in changes in both $\delta^{18}O$ and $\Delta^{17}O$ air of O_2dissolved in water. Differences in purification technique may lead to subtle fractionations between laboratories. Top panel shows all data. The bottom panel is a zoom in of $\delta^{18}O$ from 0.5 to 0.75‰. Data from ‘others’ is given in Keedakkadan and Abe (2015).

A.2. Details of regressions used to calculate $^{18}\varepsilon$ and λ values

All regressions were least-squares linear regressions. For regressions of data to Eq. (5), which is done to derive the $^{18}\varepsilon$ values, all data were normalized to the initial $\delta^{18}O$ and $\delta O_2/Ar$ of the media used in the experiments. In other words, an aliquot of the media was used to define the starting $\delta^{18}O$ and $\delta O_2/Ar$ values for each experiment. It is therefore assumed that for every experiment, all aliquots of media (i.e., each of the 500 ml Wheaton bottles subsampled from a common 5 L bottle of media) shared identical starting $\delta^{17}O$, $\delta^{18}O$, and O_2/Ar values. It follows that the intercept of the fits to Eq. (5) must pass through the origin. As such, we forced all fits through the origin. If the intercept was not forced through the origin, in all cases but one, the intercept’s value was within 2 s.e. of 0 given our analytical reproducibility (±0.05‰, 1σ) for $\delta^{18}O$ of dissolved O_2. In the one experiment where this was not the case, the intercept was found to be −0.105‰. Based on this, we consider the forcing of the intercept through the origin to be justified. We note that as we measure the O_2/Ar ratio via the ratio of the mass/charge 32 vs. 40 ion beam in the source, we are only actually constraining changes in the concentration of $^{16}O_2$. This approach is the norm in these sorts of calculations (e.g., Kiddon et al., 1993, Luz et al., 2002).

For determinations of λ values, we also required that our regressions of $\delta^{17}O$ vs. $\delta^{18}O$ based on Eq. (7) pass through the origin. We consider this acceptable as all regressions without this requirement yield intercepts within 2 s.e. of 0 based on our external reproducibility of $\Delta^{17}O$ measurements (±0.008‰, 1σ).

Before performing the regression of the data based on Eq. (7), all $\delta^{18}O$ values from individual experiments were renormalized such that a $\delta^{18}O$ of the initial media is defined to equal 0‰. $\delta^{17}O$ values were calculated for the regression using a sample’s measured $\Delta^{17}O$ and $\delta^{18}O$ values based on equation (3). This was done because $\Delta^{17}O$ values are measured with better external precision (5–10× better) than $\delta^{17}O$ values due to the occurrence of mass dependent ($\lambda \approx 0.5$) fractionations during sample preparation. Such processes can modify $\delta^{17}O$ values, but leave $\Delta^{17}O$ values largely unchanged.

The average $\Delta^{17}O$ value for O_2 dissolved in the growth medium and equilibrated with the atmosphere before *E. coli* was added was -0.001 ± 0.008 (1σ, $n = 14$). This mean and standard deviation are statistically indistinguishable (at the 1σ level) from those found for O_2dissolved in poisoned, deionized water equilibrated with the atmosphere (0.000 ± 0.008 [1σ] — see above). We interpret this similarity to indicate that

the initial $\Delta^{17}O$ values for O_2dissolved in the medium are the same as those for deionized water (within analytical precision) and thus constant for all experiments. Based on this, we used the same initial $\Delta^{17}O$ for all experiments to ensure that any imprecision in the determination of the $\Delta^{17}O$ of the media for any given experiment (which includes measurements of all incubations for the given growth conditions) does not bias the slope determined for the experiment. We used the average $\Delta^{17}O$ value determined from all measurements of media, −0.001‰, for the initial $\Delta^{17}O$ for all experiments.

A.3. Derivation of the respiration model

We modeled the isotope effects associated with the reduction of O_2 using the following simplified reaction scheme

(A1)O2⇌ikr, bindikf, bindE-O2→ikf, reduce2H2O.

In Eq. (A1), each ^{i}k refers to a rate constant for a specific reaction. *i* can be 16, 17 or, 18, indicating the rate constant associated with $^{16}O_2$, $^{16}O^{17}O$, or $^{16}O^{18}O$ respectively. E-O_2represents O_2 bound to the enzyme. We did not concern ourselves here with isotopologues with two rare isotopic species (e.g., Eiler, 2007, Yeung et al., 2012). We now derive a set of expressions to model how $^{18}\alpha$ and θ varies as a function of the relative rates of these steps. These sorts of models have been derived for other isotopic systems with different reaction pathways (e.g., Rees, 1973, Hayes, 2001, Farquhar et al., 2003), but they have not been derived for O_2 during aerobic respiration.

The isotope effects (α) associated with each of these steps are defined as:

(A2a)17ki16ki=17αi

and

(A2b)18ki16ki=18αi.

Eqs. (A2a), (A2b) can related by the mass-law slope θ [Eq. (4)] such that

(A3)17αi=18αiθ.

Here we make the typical assumption in enzyme kinetics that the concentration of E-O_2 is constant with respect to time (Briggs and Haldane, 1925, Berg et al., 2002). Under this assumption the gross flux (moles/sec) of oxygen binding to the enzyme, $\varphi_{binding}$ is equal to the sum of the O_2 unbinding from the enzyme ($\varphi_{binding}$) and being reduced ($\varphi_{being\ reduced}$).

Based on the conservation of mass, we can write the following two equations:

(A4)φbind=φunbind+φreduce.

and

(A5)φbind[iO]binding=φunbind[iO]unbinding+φreduce[iO]beingreduced

where [^{i}O] is the concentration of an isotope of O (relative to the other oxygen isotopes) with *i* representing ^{16}O, ^{17}O, or ^{18}O. We define the reversibility, r, of the binding vs. unbinding of O_2 to and from the enzyme as:

(A6)r=φunbindφbind.

Based on Eqs. (A2a), (A2b), (A3), (A4), (A5), (A6), we can write the following equation under the common assumption that ^{18}R and ^{17}R closely approximate the concentrations of ^{18}O and ^{17}O relative to all oxygen isotopes (Criss, 1999):

(A7)18αbind18RO2=r18αunbind18αreduce18RO2reduced+18αreduce(1-r)18RO2reduced,

where $^{18}R_{O2}$ is the $^{18}O/^{16}O$ ratio of O_2 in the growth medium and $^{18}R_{O2\ reduced}$ is the isotopic composition of O_2 that is being consumed by respiration. What we measure in our experiments is the 'net' fractionation between all of the steps that lead to the reduction of O_2in the medium to water, which we define as $\alpha_{measured}$ and is the α given in Eq. (5) and Table 1. $^{18}\alpha_{measured}$ is related to terms in Eq. (A7) as follows:

(A8)18αmeasured=18RO2reduced18RO2.

Combination of Eqs. (A7), (A8) gives:

(A9)18αmeasured=18αbindr18αunbind18αreduce+1-r.

A similar equation for $^{17}\alpha_{measured}$ can also be derived:

(A10)17αmeasured=18αbindθbindr18αunbindθunbind18αreduceθreduce+1-r.

From Eqs. (A9), (A10), the measured mass law slope from the experiments, $\theta_{measured}$, can be calculated:

(A11)θmeasured=ln17αmeasuredln18αmeasured

Finally, we note that although diffusion of O_2 into the cell could also be a rate-limiting step in our experiments, we consider this unlikely for two reasons. First, exponential growth is maintained in all experiments. When growth is limited by diffusion of O_2 into the cell, cell densities do not increase exponentially with time, but instead growth rates are directly proportional to the concentration of the rate-limiting nutrient (Fuchs and Kroger, 1999), which for O_2, declines in concentration over the course of an experiment. Second, if diffusion of O_2in the cell were partially rate limiting (along with O_2 reduction), we would expect that the observed isotopic fractionation for respiration in a given experiment would change as O_2concentrations decline and diffusion becomes more limiting. The result would be curvature in the plot of $\delta^{18}O$ vs. the change in O_2 concentration, which is not seen (e.g., Fig. 2, Fig. 3).

References

Angert et al., 2003

A. Angert, S. Rachmilevitch, E. Barkan, B. Luz**Effects of photorespiration, the cytochrome pathway, and the alternative pathway on the triple isotopic composition of atmospheric O_2**

Global Biogeochem. Cycles, 17 (2003)

Barkan and Luz, 2003

E. Barkan, B. Luz**High-precision measurements of $^{17}O/^{16}O$ and $^{18}O/^{16}O$ of O_2 and O_2/Ar ratio in air**

Rapid Commun. Mass Spectrom., 17 (2003), pp. 2809-2814

Barkan and Luz, 2005

E. Barkan, B. Luz**High precision measurements of $^{17}O/^{16}O$ and $^{18}O/^{16}O$ ratios in H_2O**

Rapid Commun. Mass Spectrom., 19 (2005), pp. 3737-3742

Bender et al., 1994a

M. Bender, T. Sowers, M.-L. Dickson, J. Orchardo, P. Grootes, P.A. Mayewski, D.A. Meese**Climate correlations between Greenland and Antarctica during the past 100,000 years**

Nature, 372 (1994), pp. 663-666

Bender et al., 1994b

M. Bender, T. Sowers, L. Labeyrie**The Dole effect and its variations during the last 130,000 years as measured in the Vostok ice core**

Global Biogeochem. Cycles, 8 (1994), pp. 363-376

Bender, 1990

M.L. Bender**The $\delta^{18}O$ of dissolved O_2 in seawater: A unique tracer of circulation and respiration in the deep sea**

J. Geophys. Res. Oceans, 1978–2012 (95) (1990), pp. 22243-22252

Bender and Grande, 1987

M.L. Bender, K.D. Grande**Production, respiration, and the isotope geochemistry of O_2 in the upper water column**

Global Biogeochem. Cycles, 1 (1987), pp. 49-59

Benson and Krause, 1984

B.B. Benson, D. Krause**The concentration and isotopic fractionation of oxygen dissolved in freshwater and seawater in equilibrium with the atmosphere**

Limnol. Oceanogr., 29 (1984), pp. 620-632

Berg et al., 2002

Berg, J.M., Tymoczko, J.L., Stryer, L., 2002. Biochemistry. New York.

Bigeleisen and Wolfsberg, 1958

J. Bigeleisen, M. Wolfsberg**Theoretical and experimental aspects of isotope effects in chemical kinetics**

Adv. Chem. Phys. (1958), pp. 15-76

Blunier et al., 2002

T. Blunier, B. Barnett, M.L. Bender, M.B. Hendricks**Biological oxygen productivity during the last 60,000 years from triple oxygen isotope measurements**

Global Biogeochem. Cycles, 16 (2002)

Borisov et al., 2011

V.B. Borisov, R.B. Gennis, J. Hemp, M.I. Verkhovsky**The cytochrome *bd* respiratory oxygen reductases**

Biochim. Biophys. Acta (BBA)-Bioenergetics, 1807 (2011), pp. 1398-1413

Briggs and Haldane, 1925

G.E. Briggs, J.B.S. Haldane**A note on the kinetics of enzyme action**

Biochem. J, 19 (1925), p. 338

Buchwald and Casciotti, 2010

C. Buchwald, K.L. Casciotti**Oxygen isotopic fractionation and exchange during bacterial nitrite oxidation**

Limnol. Oceanogr., 55 (2010), pp. 1064-1074

Cao and Liu, 2011

X. Cao, Y. Liu**Equilibrium mass-dependent fractionation relationships for triple oxygen isotopes**

Geochim. Cosmochim. Acta, 75 (2011), pp. 7435-7445

Casciotti et al., 2010

K.L. Casciotti, M. McIlvin, C. Buchwald**Oxygen isotopic exchange and fractionation during bacterial ammonia oxidation**

Limnol. Oceanogr., 55 (2010), pp. 753-762

Cheah et al., 2014

M.H. Cheah, A.H. Millar, R.C. Myers, D.A. Day, J. Roth, W. Hillier, M.R. Badger**Online oxygen kinetic isotope effects using membrane inlet mass spectrometry can differentiate between oxidases for mechanistic studies and calculation of their contributions to oxygen consumption in whole tissues**

Anal. Chem., 86 (2014), pp. 5171-5178

Craig and Hayward, 1987

H. Craig, T. Hayward**Oxygen supersaturation in the ocean: Biological versus physical contributions**

Science, 235 (1987), pp. 199-203

Criss, 1999

R.E. Criss**Principles of Stable Isotope Distribution**

Oxford University Press, New York (1999)

Dauphas and Schauble, 2016

N. Dauphas, E.A. Schauble**Mass fractionation laws, mass-independent effects, and isotopic anomalies**

Annu. Rev. Earth Planet. Sci., 44 (2016), pp. 709-783

del Giorgio and Duarte, 2002

P.A. del Giorgio, C.M. Duarte**Respiration in the open ocean**

Nature, 420 (2002), p. 379

Eiler, 2007

J.M. Eiler**“Clumped-isotope” geochemistry - The study of naturally-occurring, multiply-substituted isotopologues**

Earth Planet. Sci. Lett., 262 (2007), pp. 309-327

Eisenstadt et al., 2010

D. Eisenstadt, E. Barkan, B. Luz, A. Kaplan**Enrichment of oxygen heavy isotopes during photosynthesis in phytoplankton**

Photosynth. Res., 103 (2010), pp. 97-103

Emerson et al., 1995

S. Emerson, P. Quay, C. Stump, D. Wilbur, R. Schudlich**Chemical tracers of productivity and respiration in the subtropical Pacific Ocean**

J. Geophys. Res. Oceans, 100 (1995), pp. 15873-15887

Epstein and Zeiri, 1988

S. Epstein, L. Zeiri**Oxygen and carbon isotopic compositions of gases respired by humans**

Proc. Natl. Acad. Sci., 85 (1988), pp. 1727-1731

Farquhar et al., 1989

G.D. Farquhar, J.R. Ehleringer, K.T. Hubick**Carbon isotope discrimination and photosynthesis**

Annu. Rev. Plant Biol., 40 (1989), pp. 503-537

Farquhar et al., 2003

J. Farquhar, D.T. Johnston, B.A. Wing, K.S. Habicht, D.E. Canfield, S. Airieau, M.H.Thiemens**Multiple sulphur isotopic interpretations of biosynthetic pathways: implications for biological signatures in the sulphur isotope record**

Geobiology, 1 (2003), pp. 27-36

Fuchs and Kroger, 1999

G. Fuchs, A. Kroger**Growth and nutrition**

J. Lengeler, G. Drews, H.G. Schlegel (Eds.), Biology of the Prokaryotes, Blackwell Science, Oxford, UK(1999), pp. 88-109

Garcia and Gordon, 1992

H.E. Garcia, L.I. Gordon**Oxygen solubility in seawater: Better fitting equations**

Limnol. Oceanogr., 37 (1992), pp. 1307-1312

Glueckauf, 1951

E. Glueckauf**The composition of atmospheric air**

Compend. Meteorol. (1951), pp. 3-10

Guy et al., 1987

R.D. Guy, M.F. Fogel, J.A. Berry, T.C. Hoering**Isotope Fractionation During Oxygen Production and Consumption by Plants, Progress in Photosynthesis research**

Springer (1987), pp. 597-600

Guy et al., 1989

R.D. Guy, J.A. Berry, M.L. Fogel, T.C. Hoering**Differential fractionation of oxygen isotopes by cyanide-resistant and cyanide-sensitive respiration in plants**

Planta, 177 (1989), pp. 483-491

Guy et al., 1993

R.D. Guy, M.L. Fogel, J.A. Berry**Photosynthetic fractionation of the stable isotopes of oxygen and carbon**

Plant Physiol., 101 (1993), pp. 37-47

Hahnke et al., 2014

S.M. Hahnke, P. Moosmann, T.J. Erb, M. Strous**An improved medium for the anaerobic growth of Paracoccus denitrificans Pd1222**

Front. Microbiol., 5 (2014)

Han et al., 2011

H. Han, J. Hemp, L.A. Pace, H. Ouyang, K. Ganesan, J.H. Roh, F. Daldal, S.R. Blanke, R.B.Gennis**Adaptation of aerobic respiration to low O_2 environments**

Proc. Natl. Acad. Sci., 108 (2011), pp. 14109-14114

Hayes, 2001

J.M. Hayes**Fractionation of carbon and hydrogen isotopes in biosynthetic processes**

Rev. Mineral. Geochem., 43 (2001), pp. 225-277

Hayles et al., 2018

J. Hayles, C. Gao, X. Cao, Y. Liu, H. Bao**Theoretical calibration of the triple oxygen isotope thermometer**

Geochim. Cosmochim. Acta, 235 (2018), pp. 237-245

Helman et al., 2005

Y. Helman, E. Barkan, D. Eisenstadt, B. Luz, A. Kaplan**Fractionation of the three stable oxygen isotopes by oxygen-producing and oxygen-consuming reactions in photosynthetic organisms**

Plant Physiol., 138 (2005), pp. 2292-2298

Hendricks et al., 2004

M.B. Hendricks, M.L. Bender, B.A. Barnett**Net and gross O_2 production in the Southern Ocean from measurements of biological O_2saturation and its triple isotope composition**

Deep Sea Res. Part I: Oceanogr. Res. Papers, 51 (2004), pp. 1541-1561

Hendricks et al., 2005

M.B. Hendricks, M.L. Bender, B.A. Barnett, P. Strutton, F.P. Chavez**Triple oxygen isotope composition of dissolved O_2 in the equatorial Pacific: A tracer of mixing, production, and respiration**

J. Geophys. Res.: Oceans, 110 (2005)

Hoffmann et al., 2004

G. Hoffmann, M. Cuntz, C. Weber, P. Ciais, P. Friedlingstein, M. Heimann, J. Jouzel, J.Kaduk, E. Maier-Reimer, U. Seibt**A model of the Earth's Dole effect**

Global Biogeochem. Cycles, 18 (2004)

Hofmann et al., 2012

M.E. Hofmann, B. Horváth, A. Pack**Triple oxygen isotope equilibrium fractionation between carbon dioxide and water**

Earth Planet. Sci. Lett., 319 (2012), pp. 159-164

Horibe et al., 1973

Y. Horibe, K. Shigehara, Y. Takakuwa**Isotope separation factor of carbon dioxide-water system and isotopic composition of atmospheric oxygen**

J. Geophys. Res., 78 (1973), pp. 2625-2629

Johnson and Goody, 2011

K.A. Johnson, R.S. Goody**The original Michaelis constant: translation of the 1913 Michaelis-Menten paper**

Biochemistry, 50 (2011), pp. 8264-8269

Keedakkadan and Abe, 2015

H.R. Keedakkadan, O. Abe**Cryogenic separation of an oxygen–argon mixture in natural air samples for the determination of isotope and molecular ratios**

Rapid Commun. Mass Spectrom., 29 (2015), pp. 775-781

Kiddon et al., 1993

J. Kiddon, M.L. Bender, J. Orchardo, D.A. Caron, J.C. Goldman, M. Dennett**Isotopic fractionation of oxygen by respiring marine organisms**

Global Biogeochem. Cycles, 7 (1993), pp. 679-694

Kim and O'Neil, 1997

S.T. Kim, J.R. O'Neil**Equilibrium and nonequilibrium oxygen isotope effects in synthetic carbonates**

Geochim. Cosmochim. Acta, 61 (1997), pp. 3461-3475

Kroopnick and Craig, 1972

P. Kroopnick, H. Craig**Atmospheric oxygen: isotopic composition and solubility fractionation**

Science, 175 (1972), pp. 54-55

Kroopnick and Craig, 1976

P. Kroopnick, H. Craig**Oxygen isotope fractionation in dissolved oxygen in the deep sea**

Earth Planet. Sci. Lett., 32 (1976), pp. 375-388

Kroopnick, 1987

P.M. Kroopnick**Oxygen 18 in dissolved oxygen**

H.G. Osfiund, H. Craig, W.S. Broecker, D. Spence (Eds.), Geosecs Atlantic, Pacific, and Indian Ocean Expeditions, U.S. Government Printing Office, Washington, D.C. (1987)

3 and 27–182

Lane and Dole, 1956

G.A. Lane, M. Dole**Fractionation of oxygen isotopes during respiration**

Science, 123 (1956), pp. 574-576

Lehmann et al., 2009

M.F. Lehmann, B. Barnett, Y. Gélinas, D. Gilbert, R.J. Maranger, A. Mucci, B. Sundby, B.Thibodeau**Aerobic respiration and hypoxia in the Lower St. Lawrence Estuary: Stable isotope ratios of dissolved oxygen constrain oxygen sink partitioning**

Limnol. Oceanogr., 54 (2009), pp. 2157-2169

Levine et al., 2009

N.M. Levine, M.L. Bender, S.C. Doney**The $\delta^{18}O$ of dissolved O_2 as a tracer of mixing and respiration in the mesopelagic ocean**

Global Biogeochem. Cycles, 23 (2009), p. GB1006

Luna et al., 2008

V.M. Luna, Y. Chen, J.A. Fee, C.D. Stout**Crystallographic studies of Xe and Kr binding within the large internal cavity of cytochrome ba 3 from Thermus thermophilus: Structural analysis and role of oxygen transport channels in the heme− Cu oxidases**

Biochemistry, 47 (2008), pp. 4657-4665

Luz and Barkan, 2000

B. Luz, E. Barkan**Assessment of oceanic productivity with the triple-isotope composition of dissolved oxygen**

Science, 288 (2000), pp. 2028-2031

Luz and Barkan, 2005

B. Luz, E. Barkan**The isotopic ratios $^{17}O/^{16}O$ and $^{18}O/^{16}O$ in molecular oxygen and their significance in biogeochemistry**

Geochim. Cosmochim. Acta, 69 (2005), pp. 1099-1110

Luz and Barkan, 2009

B. Luz, E. Barkan**Net and gross oxygen production from O_2/Ar, $^{17}O/^{16}O$ and $^{18}O/^{16}O$ ratios**

Aquat. Microb. Ecol., 56 (2009), pp. 133-145

Luz and Barkan, 2011

B. Luz, E. Barkan**The isotopic composition of atmospheric oxygen**

Global Biogeochem. Cycles, 25 (2011)

Luz et al., 1999

B. Luz, E. Barkan, M.L. Bender, M.H. Thiemens, K.A. Boering**Triple-isotope composition of atmospheric oxygen as a tracer of biosphere productivity**

Nature, 400 (1999), pp. 547-550

Luz et al., 2002

B. Luz, E. Barkan, Y. Sagi, Y.Z. Yacobi**Evaluation of community respiratory mechanisms with oxygen isotopes: A case study in Lake Kinneret**

Limnol. Oceanogr., 47 (2002), pp. 33-42

Maier-Reimer, 1993

E. Maier-Reimer**Geochemical cycles in an ocean general circulation model. Preindustrial tracer distributions**

Global Biogeochem. Cycles, 7 (1993), pp. 645-677

Matsuhisa et al., 1978

Y. Matsuhisa, J.R. Goldsmith, R.N. Clayton**Mechanisms of hydrothermal crystallization of quartz at 250 C and 15 kbar**

Geochim. Cosmochim. Acta, 42 (1978), pp. 173-182

McNaught and Wilkinson, 1997

A.D. McNaught, A. Wilkinson**Compendium of Chemical Terminology: IUPAC Recommendations**

(2nd ed.), Blackwell Science, Oxford, England (1997)

Miller, 2002

M.F. Miller**Isotopic fractionation and the quantification of 17 O anomalies in the oxygen three-isotope system: an appraisal and geochemical significance**

Geochim. Cosmochim. Acta, 66 (2002), pp. 1881-1889

Morris and Schmidt, 2013

R.L. Morris, T.M. Schmidt**Shallow breathing: bacterial life at low O_2**

Nat. Rev. Microbiol., 11 (2013), pp. 205-212

Nakayama et al., 2007

N. Nakayama, H. Obata, T. Gamo**Consumption of dissolved oxygen in the deep Japan Sea, giving a precise isotopic fractionation factor**

Geophys. Res. Lett., 34 (2007)

Naqui et al., 1986

A. Naqui, B. Chance, E. Cadenas**Reactive oxygen intermediates in biochemistry**

Annu. Rev. Biochem., 55 (1986), pp. 137-166

Nicholson et al., 2014

D. Nicholson, R.H. Stanley, S.C. Doney**The triple oxygen isotope tracer of primary productivity in a dynamic ocean model**

Global Biogeochem. Cycles, 28 (2014), pp. 538-552

Petit et al., 1999

J.-R. Petit, J. Jouzel, D. Raynaud, N.I. Barkov, J.-M. Barnola, I. Basile, M. Bender, J.Chappellaz, M. Davis, G. Delaygue**Climate and atmospheric history of the past 420,000 years from the Vostok ice core, Antarctica**

Nature, 399 (1999), pp. 429-436

Quay et al., 1993

P. Quay, S. Emerson, D. Wilbur, C. Stump, M. Knox**The $\delta^{18}O$ of dissolved O_2 in the surface waters of the subarctic Pacific: a tracer of biological productivity**

J. Geophys. Res. Oceans, 98 (1993), pp. 8447-8458

Ratkowsky et al., 1982

D. Ratkowsky, J. Olley, T. McMeekin, A. Ball**Relationship between temperature and growth rate of bacterial cultures**

J. Bacteriol., 149 (1982), pp. 1-5

Rees, 1973

C. Rees**A steady-state model for sulphur isotope fractionation in bacterial reduction processes**

Geochim. Cosmochim. Acta, 37 (1973), pp. 1141-1162

Reuer et al., 2007

M.K. Reuer, B.A. Barnett, M.L. Bender, P.G. Falkowski, M.B. Hendricks**New estimates of Southern Ocean biological production rates from O_2/Ar ratios and the triple isotope composition of O_2**

Deep Sea Res. Part I: Oceanogr. Res. Papers, 54 (2007), pp. 951-974

Ribas-Carbo et al., 1995

M. Ribas-Carbo, J.A. Berry, D. Yakir, L. Giles, S.A. Robinson, A.M. Lennon, J.N.Siedow**Electron partitioning between the cytochrome and alternative pathways in plant mitochondria**

Plant Physiol., 109 (1995), pp. 829-837

Rice and Hempfling, 1978

C.W. Rice, W.P. Hempfling**Oxygen-limited continuous culture and respiratory energy conservation in Escherichia coli**

J. Bacteriol., 134 (1978), pp. 115-124

Robinson et al., 1992

S.A. Robinson, D. Yakir, M. Ribas-Carbo, L. Giles, C.B. Osmond, J.N. Siedow, J.A. Berry**Measurements of the engagement of cyanide-resistant respiration in the Crassulacean acid metabolism plant Kalanchoe daigremontiana with the use of on-line oxygen isotope discrimination**

Plant Physiol., 100 (1992), pp. 1087-1091

Sarmiento and Gruber, 2006

J.L. Sarmiento, N. Gruber**Ocean Biogeochemical Dynamics**

Princeton University Press, Princeton, NJ (2006)

Savenkoff et al., 1996

C. Savenkoff, A. Vézina, T. Packard, N. Silverberg, J.-C. Therriault, W. Chen, C. Bérubé, A. Mucci, B. Klein, F. Mesplé**Distributions of oxygen, carbon, and respiratory activity in the deep layer of the Gulf of St. Lawrence and their implications for the carbon cycle**

Can. J. Fish. Aquat. Sci., 53 (1996), pp. 2451-2465

Schleser, 1979

G. Schleser**Oxygen isotope fractionation during respiration for different temperatures of T. utilis and E. coli K12**

Radiat. Environ. Biophys., 17 (1979), pp. 85-93

Severinghaus et al., 2009

J.P. Severinghaus, R. Beaudette, M.A. Headly, K. Taylor, E.J. Brook**Oxygen-18 of O_2 records the impact of abrupt climate change on the terrestrial biosphere**

Science, 324 (2009), pp. 1431-1434

Sharp et al., 2016

Z. Sharp, J. Gibbons, O. Maltsev, V. Atudorei, A. Pack, S. Sengupta, E. Shock, L. Knauth**A calibration of the triple oxygen isotope fractionation in the SiO_2–H_2O system and applications to natural samples**

Geochim. Cosmochim. Acta, 186 (2016), pp. 105-119

Stern et al., 1968

M.J. Stern, W. Spindel, E. Monse**Temperature dependences of isotope effects**

J. Chem. Phys., 48 (1968), p. 2908

Stevens et al., 1975

C.L. Stevens, D. Schultz, C. Van Baalen, P.L. Parker**Oxygen isotope fractionation during photosynthesis in a blue-green and a green alga**

Plant Physiol., 56 (1975), pp. 126-129

Tian and Klinman, 1993

G. Tian, J.P. Klinman**Discrimination between ^{16}O and ^{18}O in oxygen binding to the reversible oxygen carriers hemoglobin, myoglobin, hemerythrin, and hemocyanin: a new probe for oxygen binding and reductive activation by proteins**

J. Am. Chem. Soc., 115 (1993), pp. 8891-8897

Urey, 1947

H.C. Urey**The thermodynamic properties of isotopic substances**

J. Chem. Soc. (1947), pp. 562-581

Valentine et al., 2004

D.L. Valentine, A. Chidthaisong, A. Rice, W.S. Reeburgh, S.C. Tyler**Carbon and hydrogen isotope fractionation by moderately thermophilic methanogens**

Geochim. Cosmochim. Acta, 68 (2004), pp. 1571-1590

Weiss, 1970

R. Weiss**The Solubility of Nitrogen, Oxygen and Argon in Water and Seawater, Deep Sea Research and Oceanographic Abstracts**

Elsevier (1970), pp. 721-735

Wikström, 2006

M. Wikström**Cytochrome Oxidase**

Wiley Online Library (2006)

Yeung et al., 2012

L.Y. Yeung, E.D. Young, E.A. Schauble**Measurements of $^{18}O^{18}O$ and $^{17}O^{18}O$ in the atmosphere and the role of isotope-exchange reactions**

J. Geophys. Res., 117 (2012), 10.1029/2012JD017992

Yoshinaga et al., 2014

M.Y. Yoshinaga, T. Holler, T. Goldhammer, G. Wegener, J.W. Pohlman, B. Brunner, M.M.Kuypers, K.-U. Hinrichs, M. Elvert**Carbon isotope**

equilibration during sulphate-limited anaerobic oxidation of methane

Nat. Geosci. (2014)

Young et al., 2002

E.D. Young, A. Galy, H. Nagahara**Kinetic and equilibrium mass-dependent isotope fractionation laws in nature and their geochemical and cosmochemical significance**

Geochim. Cosmochim. Acta, 66 (2002), pp. 1095-1104

Zanconato et al., 1992

S. Zanconato, D.M. Cooper, Y. Armon, S. Epstein**Effect of increased metabolic rate on oxygen isotopic fractionation**

Respir. Physiol., 89 (1992), pp. 319-327

[1] $\delta^{i}O = {}^{i}R_{sample}/{}^{i}R_{standard}$ where $R = [{}^{i}O]/[{}^{16}O]$, brackets denote concentrations, and *i* can be either 17 or 18. The standard to which all measurements are referred to in this paper (i.e., that have $\delta^{17}O$ and $\delta^{18}O$ equal to 0‰) is tropospheric air.

[2] $\delta O_2/Ar$ is defined as follows: $1000 \times ([{}^{32}O_2/{}^{40}Ar_{sample}/{}^{32}O_2/{}^{40}Ar_{air}] - 1)$.